

Simulation Scenarios in One-Dimensional Self-Gravitating System

A guided study for the partial fulfillment of Ph.D. coursework

by

Suman Pramanick

Advisor

Somnath Bharadwaj

Department of Physics

Indian Institute of Technology Kharagpur
Kharagpur, West Bengal 721302, India

ABSTRACT

We study and compare different numerical differential equation solvers on the basis of numerical complexity, energy conservation, and stable solution in phase-space for the Simple Harmonic Oscillation (SHM) problem. We conclude and show that the Leapfrog method is the best for our problem. We solve Poisson's equation in gravity on the computation grid by the finite difference method and Fourier method. We solve Poisson's equation for source not in a grid point by cloud-in cell method. Finally, we simulate one-dimensional self-gravitating system and show the evolution of the system via phase-space trajectories.

Contents

1	Solutions by Euler, RK-2 and RK-4 Methods	1
1.1	Aim	1
1.2	Introduction	1
1.3	Problem	2
1.4	Euler Method	2
1.4.1	Solution of SHM Problem	3
1.5	Second order Runge-Kutta method	3
1.5.1	Derivation of RK-2	4
1.5.2	Explanations of plots	7
1.6	Fourth-Order Runge-Kutta method	8
1.6.1	Iteration steps	8
1.6.2	Explanations of plots	9
1.7	Error Analysis and Discussions	10
1.8	Conclusion	12
2	Solution by Leapfrog Method	14
2.1	Aim	14
2.2	Introduction	14
2.3	Algorithm of Leapfrog Method	15
2.4	Explanation of Plots	16
2.5	Discussions and Conclusions	17
3	Solution of Poisson's Equation using Finite Difference Method	20
3.1	Aim	20
3.2	Introduction	20
3.3	Brief Theory	20

3.4	Simulation Parameters	21
3.5	Potential Plots	21
4	Fourier Method Solution of Poisson's Equation	24
4.1	Aim	24
4.2	Introduction	24
4.3	Problem Parameters	25
4.4	Explanation of Plots	25
5	Solution of Poisson's Equation by CIC Method	32
5.1	Aim	32
5.2	Introduction	32
5.3	Brief Theory	32
5.4	Simulation Parameters	33
5.5	Results and Plots	33
6	Simulation of 1D Self-Gravitating System	36
6.1	Aim	36
6.2	Introduction	36
6.3	Brief Theory	36
6.4	Simulation Parameters	37
6.5	Explanation of plots	37
6.6	Video of the simulation	37
	Bibliography	42

Chapter 1

Solutions by Euler, RK-2 and RK-4 Methods

1.1 Aim

To Solve the Simple Harmonic Oscillation (SHM) problem by Euler method, Runge-Kutta second order (RK-2) method and Runge-Kutta fourth order (RK-4) method.

1.2 Introduction

There are very few real systems which can be solve analytically, safely we can say most of the real life systems we can not solve analytically. However we can formulate the system mathematically and can write the differential equations to solve the system. These systems can be solved using numerical methods with obviously some boundary conditions specified. The solution we get from numerical techniques are not error free, because in every numerical technique we assume some simple steps to reduce the complexity of the system. Those assumptions are good approximation of the real system but not exactly the real system. That leads to a accumulation of errors in each computational steps (iterations). For a long run these errors sum up and sometime make the numerical system way deviate from the real system.

There are two things we need keep in mind. We have to take each infinitesimal steps such that they don not deviate much from the real system. The second point is to do such we cannot suggest an infinitesimal process which makes a huge computational complexity, because that will make more run time and sometimes less efficient. So,

basically we have to balance between these two things, and have to choose the most efficient technique according to our requirements.

1.3 Problem

In this assignment we will solve the simple harmonic oscillation (SHM) problem. The equations of the problem are:

$$\frac{dx}{dt} = \frac{p}{m} \text{ and } \frac{dp}{dt} = -kx \tag{1.1}$$

The parameters for our problem are:

$$k = 1; m = 1; \omega = 1 \text{ and } T = 2\pi \tag{1.2}$$

Before solving the equations with different numerical techniques we will briefly discuss about the details of some numerical techniques to solve differential equations.

1.4 Euler Method

Euler method is a first-order method of solving differential equation. The error per step in Euler method is proportional to the square of the step size. The global error of Euler method is however proportional to the step size. This is the simplest and basic method of solving differential equation.

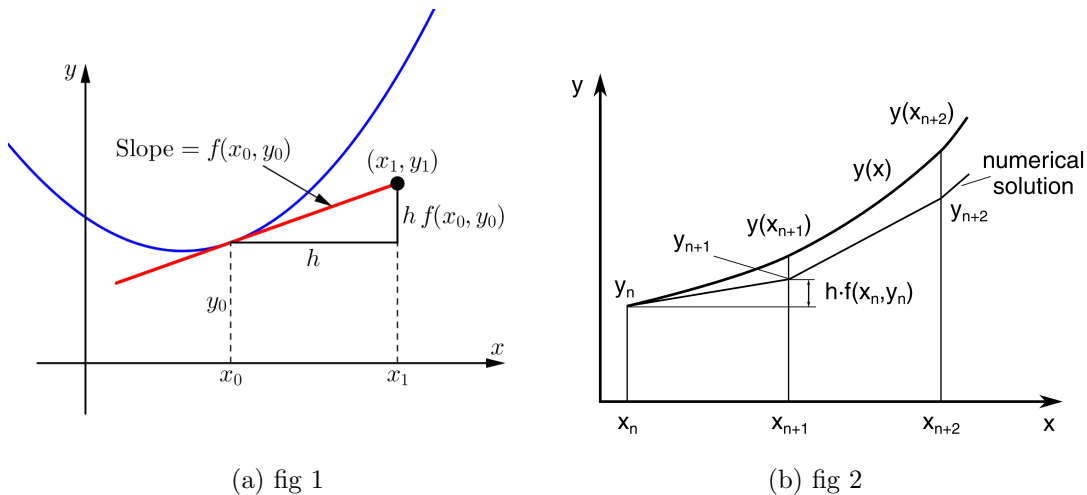


Figure 1.1: Euler method approximate solution

According to figure 1.1, we can see that at point (x_0, y_0) the slope (slope of the tangent at that point) is $\frac{dy}{dx}$. lets say $\frac{dy}{dx} = f(x, y)$ then at point (x_0, y_0) the slope is $f(x_0, y_0)$. for a small increment h we can approximate $y_0 + hf(x_0, y_0)$ as the new value of y at point $x_0 + h$. So, we can write the iterative formula as

$$x_{n+1} = x_n + h \tag{1.3}$$

$$y_{n+1} = y_n + hf(x_n, y_n) \tag{1.4}$$

So, we need the initial values of x and y to compute the whole function in iterative method. If we want other points along the path of the true solution, and yet we don't actually have the true solution, then it looks like using the tangent line as an approximation might be our best bet! After all, at least on this picture, it looks like the line stays pretty close to the curve if you don't move too far away from the initial point.

In this way according to figure 1.1 we can see that we can at least trace the function and if the step size h is very small then we can actually very accurately calculate the function.

1.4.1 Solution of SHM Problem

Now let us discuss the SHM problem which is our main goal in this chapter.

Form figure 1.2 we can see that the solution is diverging for small N values but for large N , like $N = 10000$ the solution is very close to the actual elliptical solution. For small N the step size h is very small, so error accumulation is large in each step.

The energy of the system should be constant as the system is conservative and has no damping. From figure 1.4 we can see the energy is diverging for small N . However for large N the energy is comparably constant of the process.

1.5 Second order Runge-Kutta method

Runge-Kutta methods are among the most popular ODE solvers. They were first studied by Carle Runge and Martin Kutta around 1900. In contrast to the multistep methods of the previous section, Runge-Kutta methods are single-step methods — however, with multiple stages per step. They are motivated by the dependence of the Taylor methods on the specific IVP. These new methods do not require derivatives of

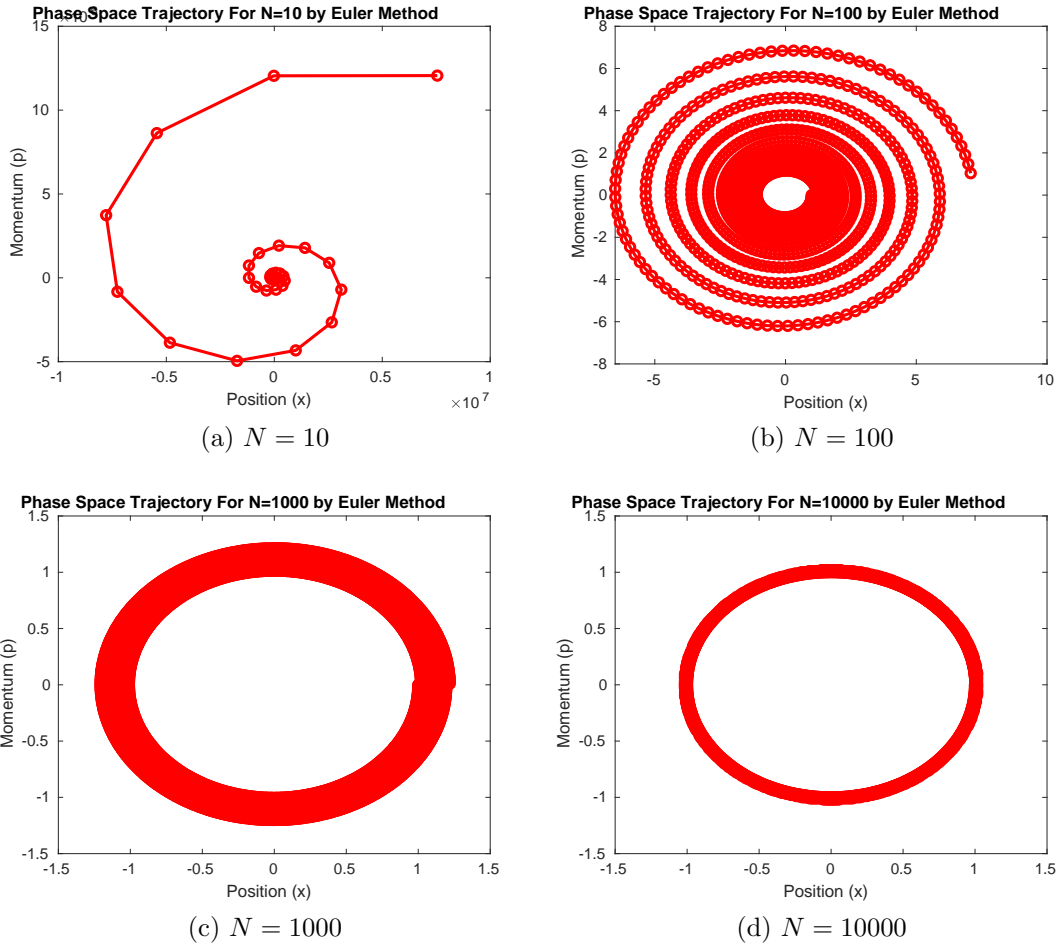


Figure 1.2: Phase space trajectories for different number of steps (N) inside a full time period T (For Euler method)

the right-hand side function f in the code, and are therefore general-purpose initial value problem solvers.

1.5.1 Derivation of RK-2

Let us consider

$$\frac{dy}{dx} = f(x, y) \quad (1.5)$$

The Taylor expansion of $y(x)$ is

$$y(x+h) = y(x) + hy'(x) + \frac{h^2}{2}y''(x) + \mathcal{O}(h^3) \quad (1.6)$$

The second derivative of y in terms of f is

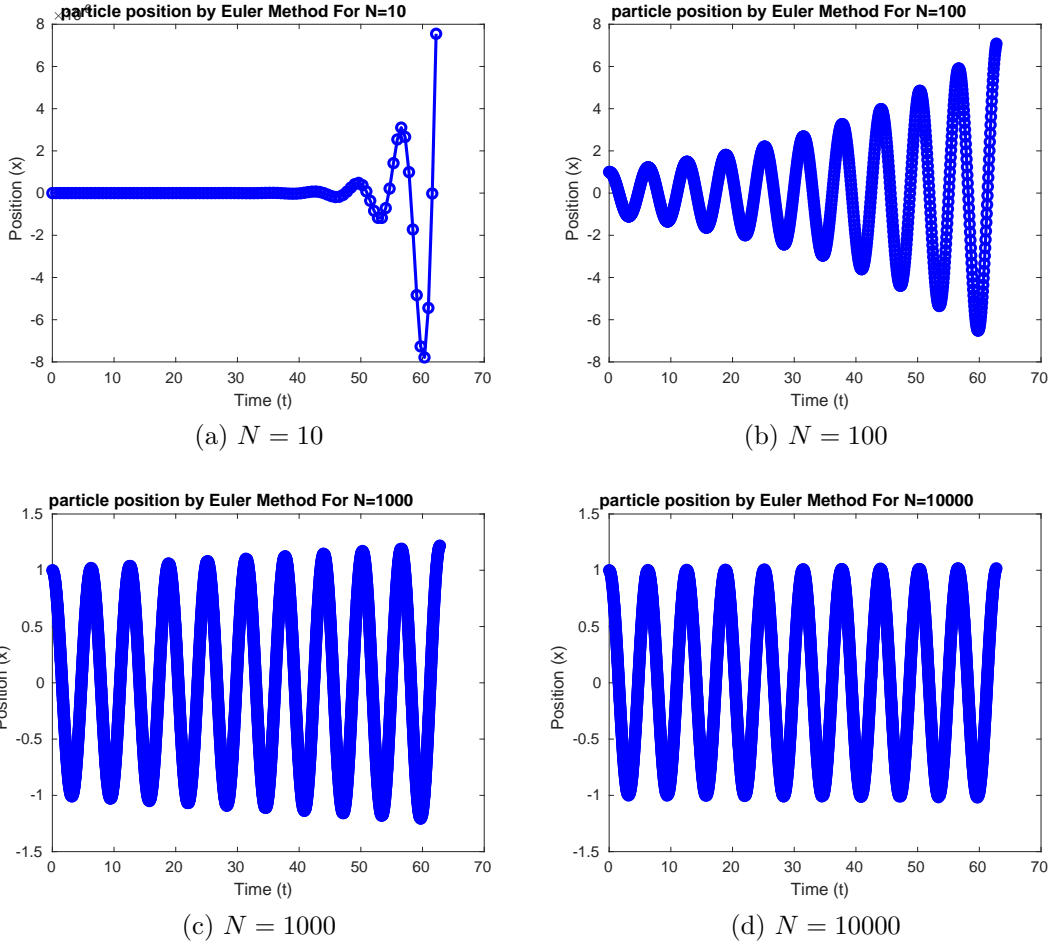


Figure 1.3: Solution of $x(t)$ vs t plot for different number of steps (N) inside a full time period T (For Euler method)

$$y''(x) = f_x(x, y) + f_y(x, y)f(x, y) \quad (1.7)$$

f_y is the Jacobian. the Taylor series expansion of y becomes

$$y(x + h) = y(x) + hf(x, y) + \frac{h^2}{2}[f_x(x, y) + f_y(x, y)f(x, y)] + \mathcal{O}(h^3) \quad (1.8)$$

$$y(x + h) = y(x) + \frac{h}{2}f(x, y) + \frac{h}{2}[f_x(x, y) + hf_x(x, y) + hf_y(x, y)f(x, y)] + \mathcal{O}(h^3) \quad (1.9)$$

From multivariate Taylor series expansion

$$f(x + h, y + k) = f(x, y) + hf_x(x, y) + f_y(x, y)k + \dots \quad (1.10)$$

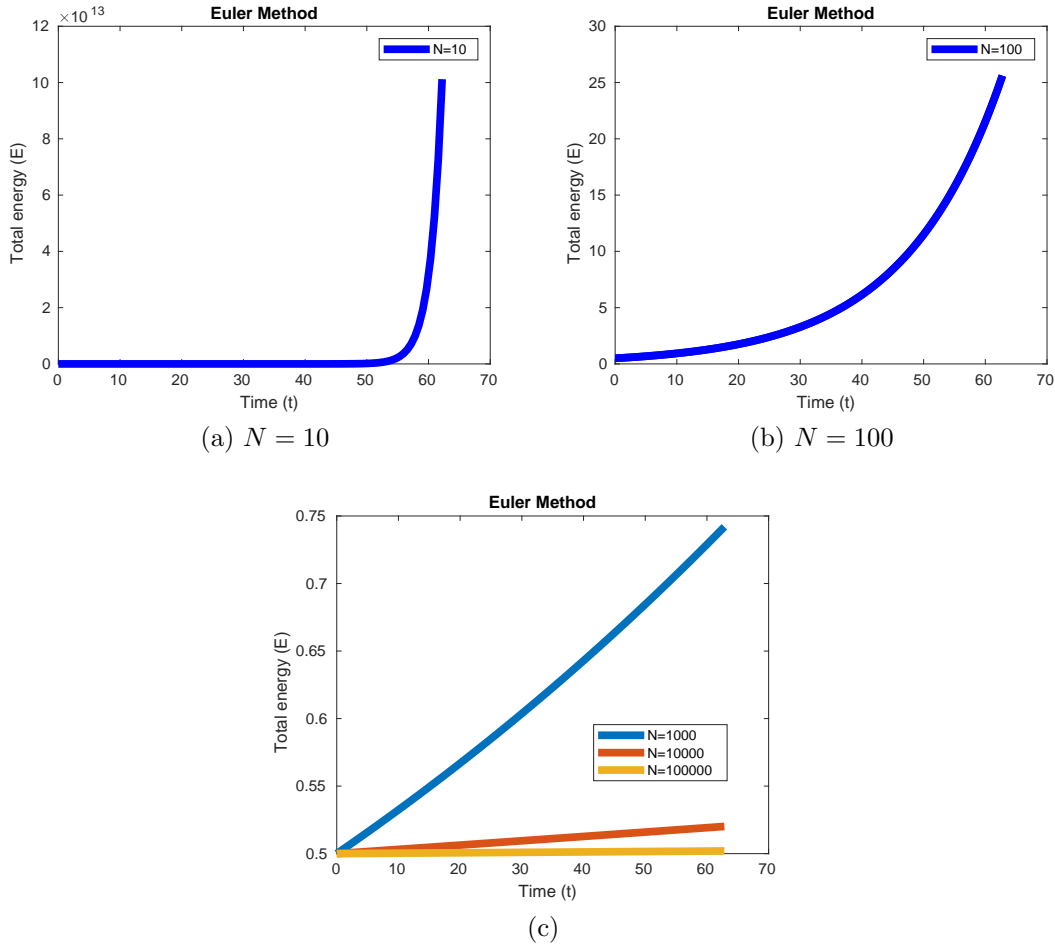


Figure 1.4: Constant energy value of the solution over time (For Euler method).

So,

$$f(x + h, y + hf(x, y)) = f(x, y) + hf_x(x, y) + hf_y(x, y)f(x, y) + \mathbf{O}(h^2) \quad (1.11)$$

Therefore, we get

$$y(x + h) = y(x) + \frac{h}{2}f(x, y) + \frac{h}{2}[f(x + h, y + hf(x, y))] + \mathcal{O}(h^3) \quad (1.12)$$

$$y_{n+1} = y_n + h \left(\frac{1}{2}k_1 + \frac{1}{2}k_2 \right)$$

Where,

$$k_1 = f(x_n, y_n) \quad (1.13)$$

$$k_2 = f(x_n + h, y_n + hk_1) \quad (1.14)$$

1.5.2 Explanations of plots

From figure 1.5 we can see for small value of N the phase space solution is diverging. However for larger values of N we get very close solution to actual elliptical one.

From figure 1.6 we can see that the solution of position $x(t)$ is diverging for small N , but for large N we get very stable solution.

The constancy of total energy value also can be observed from figure 1.7. However for small N energy value is not constant after some iteration, but for large N values it is well constant.

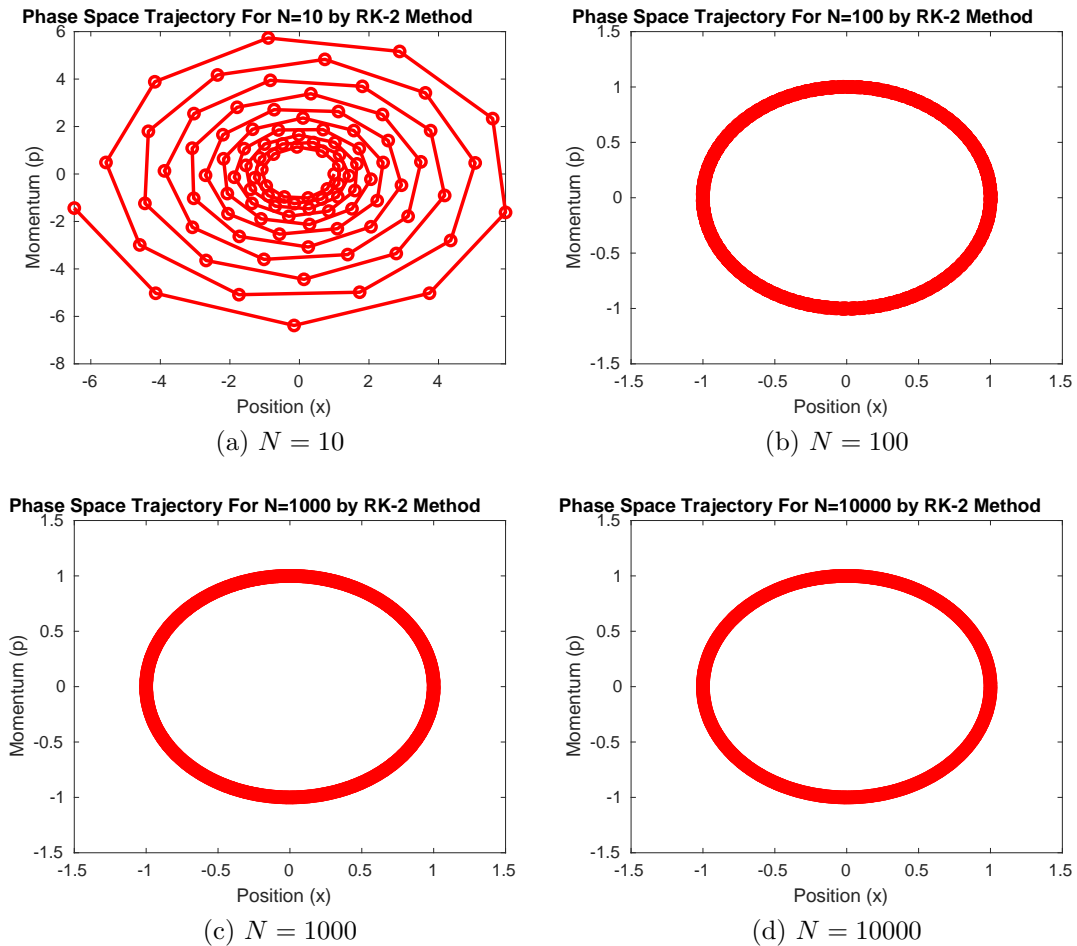


Figure 1.5: Phase space trajectories for different number of steps (N) inside a full time period T (For second-order Runge-Kutta Method)

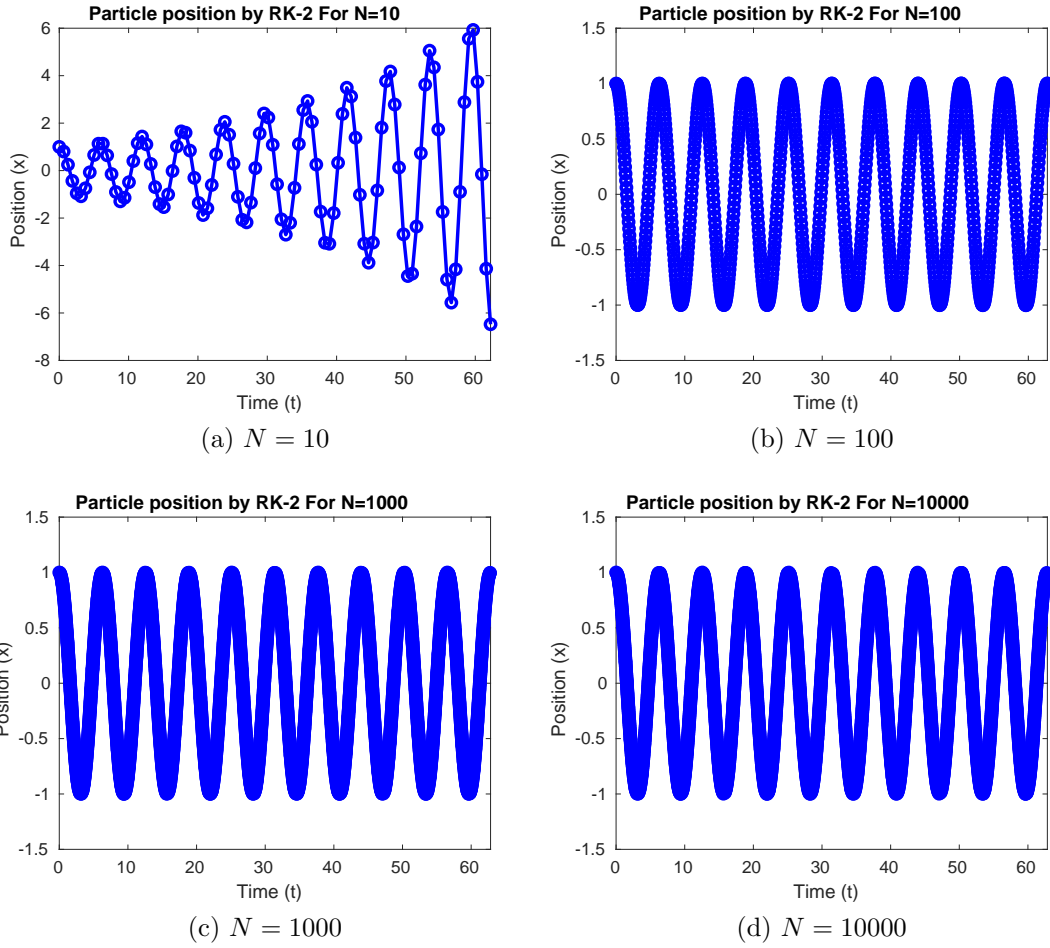


Figure 1.6: Solution of $x(t)$ vs t plot for different number of steps (N) inside a full time period T (For second-order Runge-Kutta Method)

1.6 Fourth-Order Runge-Kutta method

1.6.1 Iteration steps

The classical fourth-order Runge-Kutta Method is given by

$$y_{n+1} = y_n + h \left[\frac{k_1}{6} + \frac{k_2}{3} + \frac{k_3}{3} + \frac{k_4}{6} \right] \quad (1.15)$$

where,

$$k_1 = f(x_n, y_n) \quad (1.16)$$

$$k_2 = f \left(x_n + \frac{h}{2}, y_n + \frac{h}{2}k_1 \right) \quad (1.17)$$

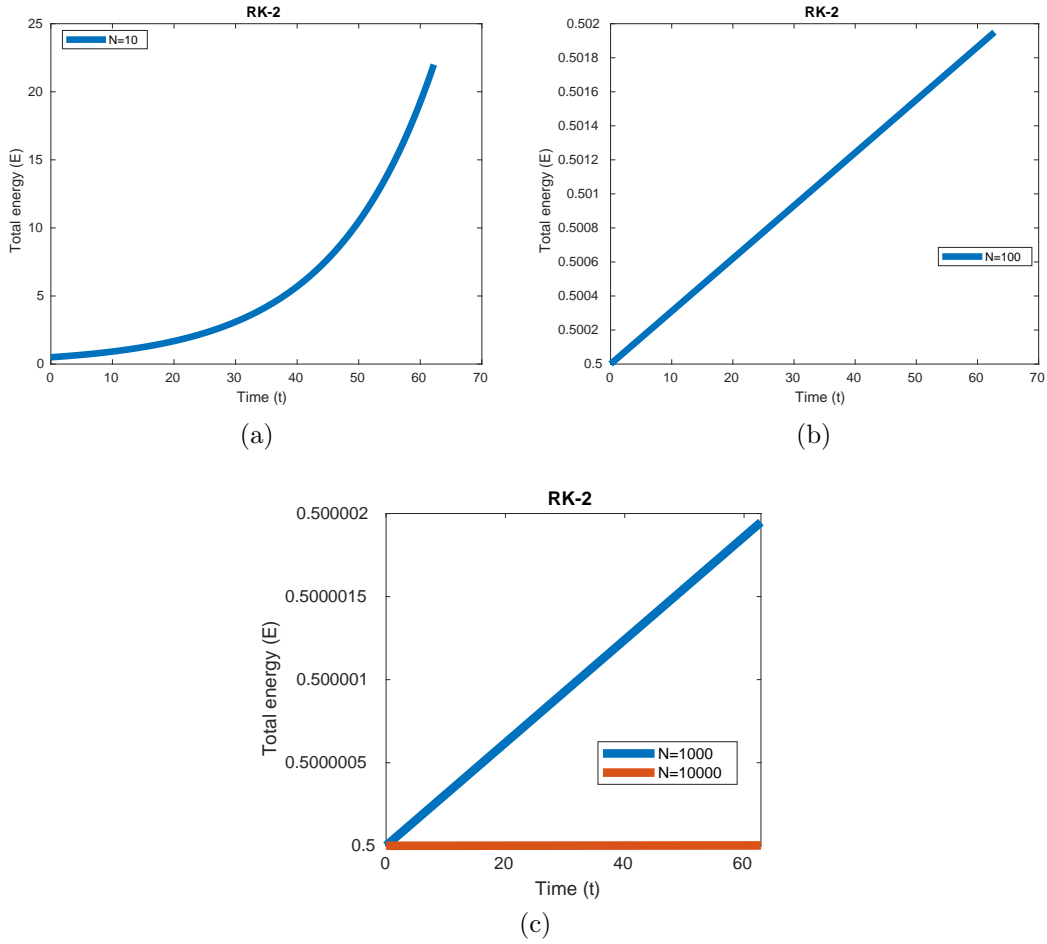


Figure 1.7: Constant energy value of the solution over time (For second-order Runge-Kutta Method)

$$k_3 = f\left(x_n + \frac{h}{2}, y_n + \frac{h}{2}k_2\right) \quad (1.18)$$

$$k_4 = f(x_n + h, y_n + hk_3) \quad (1.19)$$

1.6.2 Explanations of plots

From figure 1.8 we can see that also for very small value of N ($N = 10$) the phase space trajectory is stable and form a well ellipse.

Same thing we can see in $x(t)$ plots (figure 1.9). The solution is stable and well sinusoidal.

The constancy of energy value is very good in this method. We can see that a

very negligible energy change is there (figure 1.10) which is very less comparing to other methods.

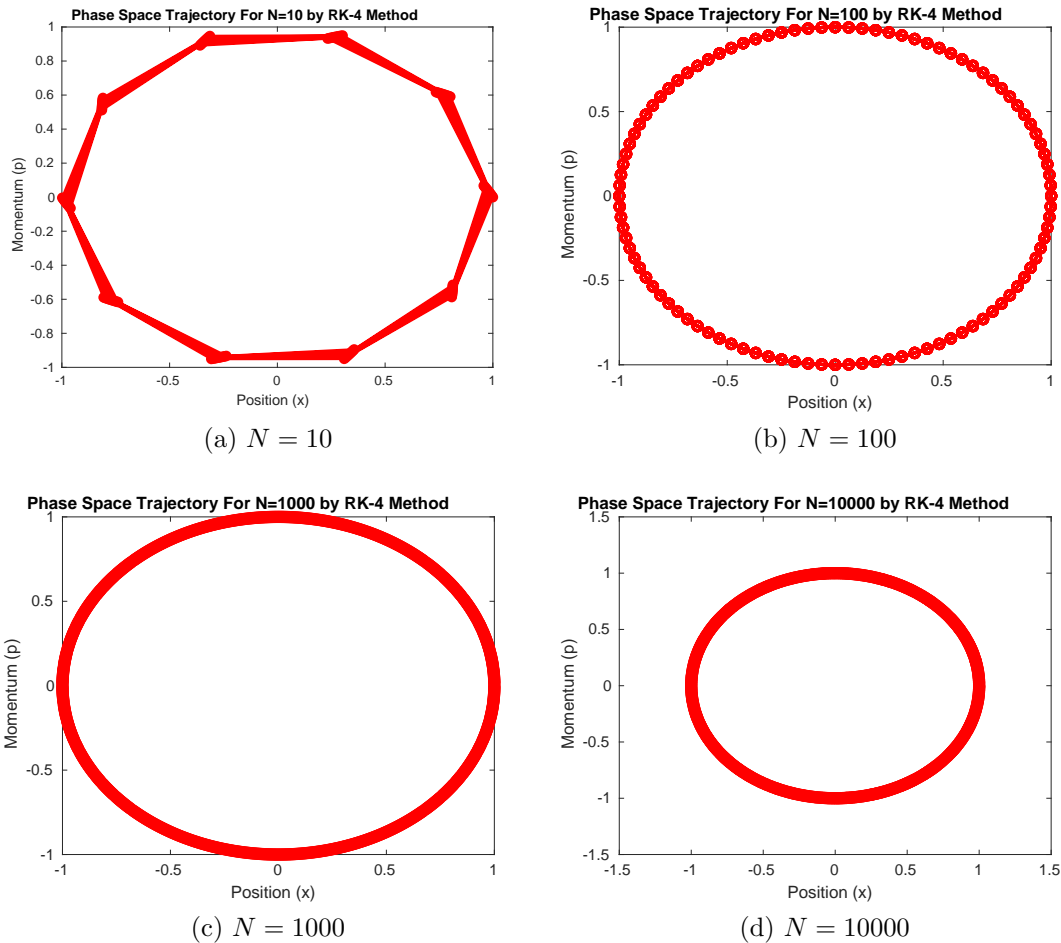


Figure 1.8: Phase space trajectories for different number of steps (N) inside a full time period T (For fourth-order Runge-Kutta Method)

1.7 Error Analysis and Discussions

From the plots we clearly can see that for a fixed number of steps N the solution is better in RK-2 method than Euler method. Again RK-4 solution is much better than RK-2 solutions. Euler method is first order method, where RK-2 is a second order method. so just by increasing an order we see that result improve much. Same thing is happening in the case of RK-2 and Rk-4 methods. RK-4 is a Fourth-order

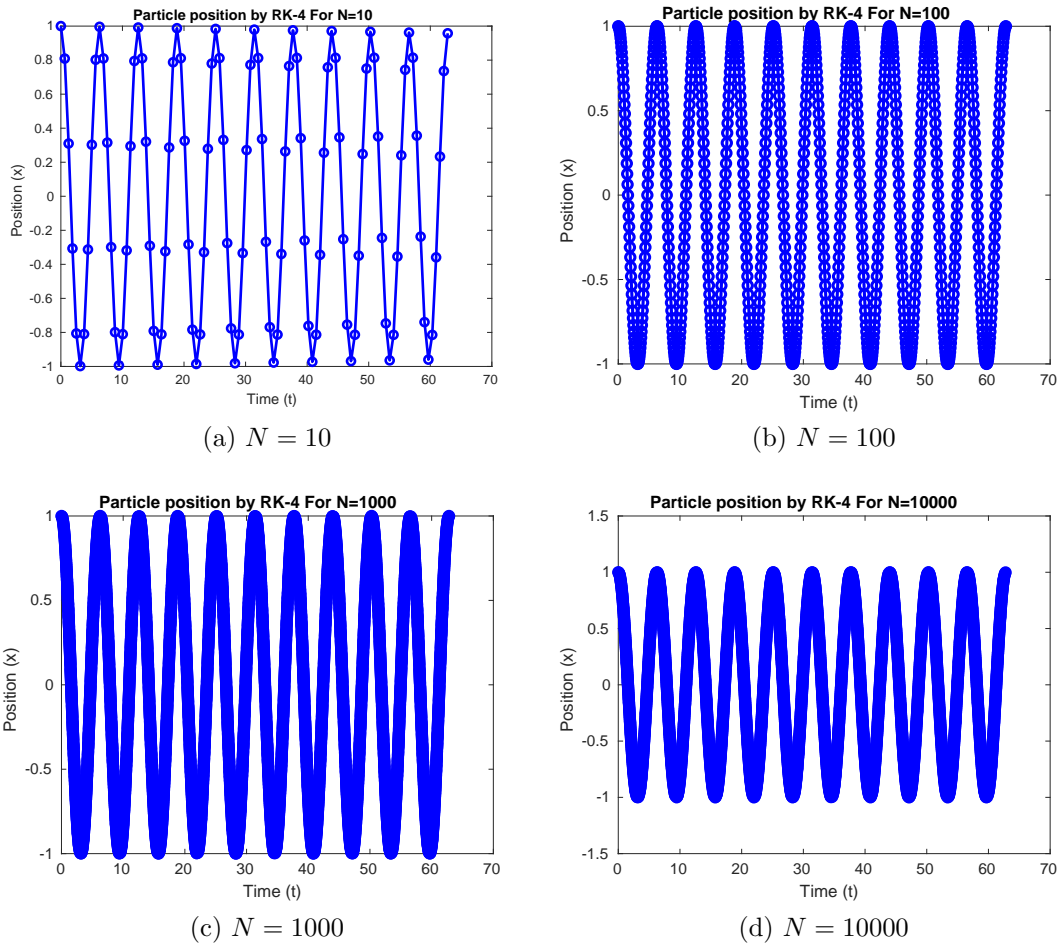


Figure 1.9: Solution of $x(t)$ vs t plot for different number of steps (N) inside a full time period T (For Fourth-order Runge-Kutta Method)

approximation whereas RK-2 is second-order. So, just by increasing two orders the error of the solution minimizes a lot. In terms of Taylor series

$$y(x+h) = y(x) + hy'(x) + \frac{h^2}{2}y''(x) + \dots \quad (1.20)$$

The Taylor series is an infinite series. computationally it is impossible to take infinite terms. If we just take two terms in the RHS, then that is a first-order approximation, which is Euler method. If we take three terms then that is a second-order approximation and it has been shown in section 1.5.1 that it is nothing but RK-2 method. Now in figure 1.11 we plotted the relative error in energy, i.e. $\varepsilon = \frac{\Delta E}{E}$ where E is the total energy of the system, which should be constant of the system

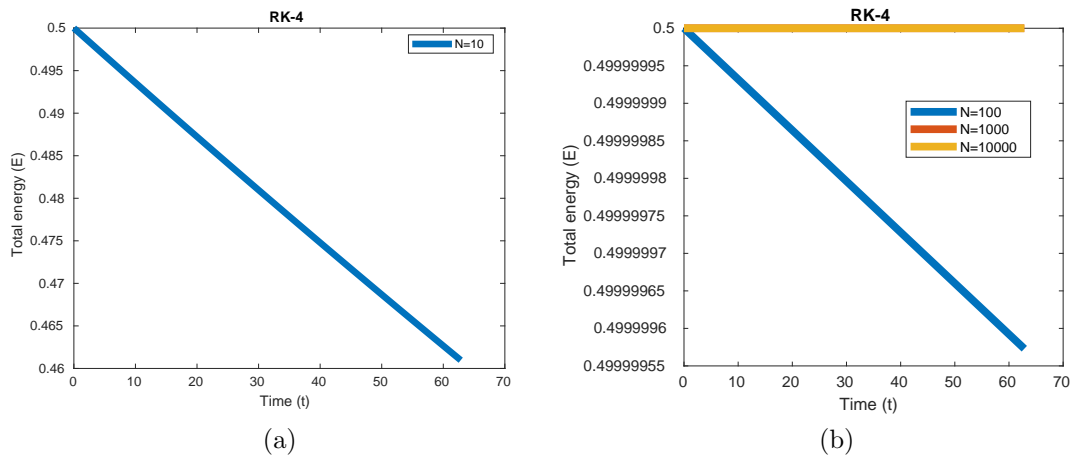


Figure 1.10: Constant energy value of the solution over time (For Fourth-order Runge-Kutta Method)

and ΔE is the energy change in the process due to accumulation of error. We plotted this relative error with respect to number of steps N in log-log scale. Theoretically $\Delta E = 0$ so we should get a line parallel to ε axis and passing through 0. But due to error accumulation in each step, the actual plot that we get for different methods is shown in figure 1.11.

From figure 1.11 it is clear for every process the error is less for larger number of steps N . The slope of the plot is however less for Euler method, RK-2 is in middle and RK-4 has maximum slope. Larger slope means the error is falling faster with N .

1.8 Conclusion

From this assignment we conclude that obviously high order methods are less erratic and error per step is also less. But for computational simplicity we cannot choose higher order methods as much as we want. So, we have choose a simple less order method but again with less error. In next chapter we will talk about such a method, which is first order but still energy conserving.

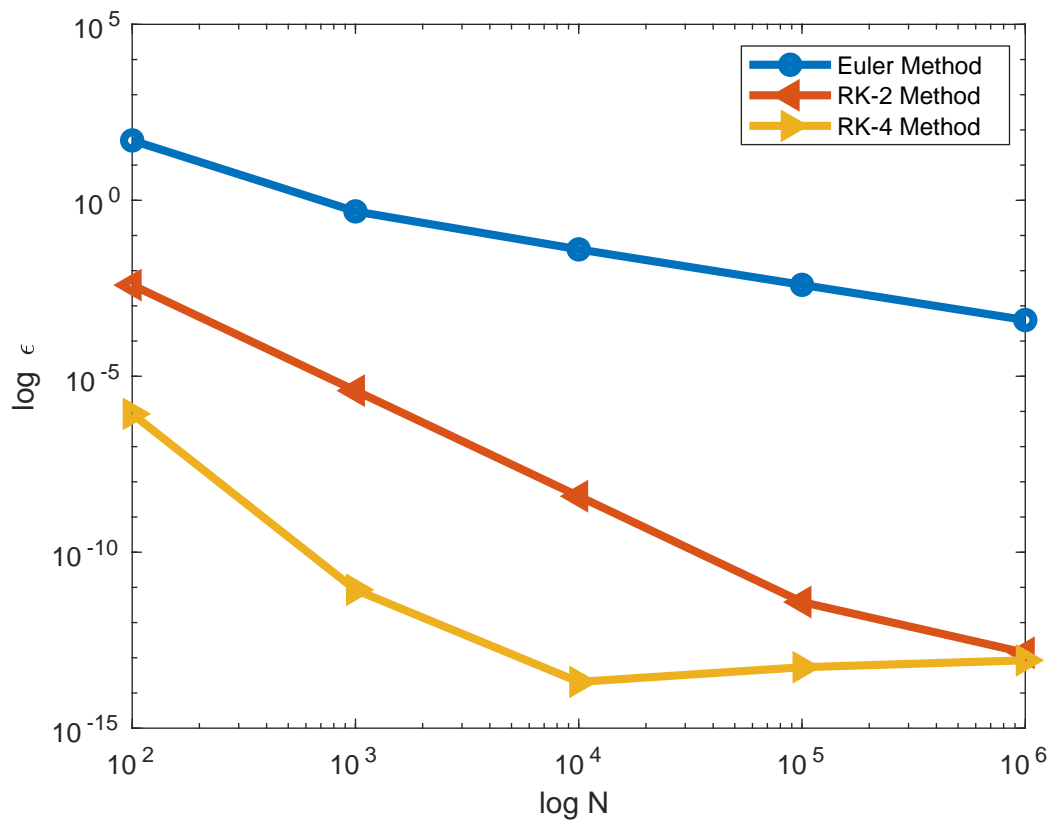


Figure 1.11: ϵ vs N plot in log-log scale for different numerical methods

Chapter 2

Solution by Leapfrog Method

2.1 Aim

To solve the SHM problem by Leap frog method and check its energy conserving and reversible properties. To compare the solution of SHM problem by Leapfrog method with solutions of the same by previously discussed methods (Euler, RK-2 and RK-4).

2.2 Introduction

Leapfrog method is a numerical differential equation solver of the form

$$\frac{d^2x}{dt^2} = a(x) \quad (2.1)$$

This second order differential equation can be written in form of a coupled first order differential equation as

$$\frac{dx}{dt} = v(x) \text{ and } \frac{dv}{dt} = a(x) \quad (2.2)$$

This method is very much useful for dynamical mechanical systems. This is a first order method, so the computational complexity is less, at the same time it is less erratic process. The accumulation of errors in energy is very less, so this process is energy conserving. For our SHM problem, the force is conservative so the energy should be constant. In previous Assignment we see that this constancy of energy is no longer retained in first order methods like Euler method. Here we will solve the same using leapfrog method and will compare our results with previous assignment (Assignment-2).

2.3 Algorithm of Leapfrog Method

We are going to solve a second order differential equation, so to solve it we need two initial conditions. The initial conditions are initial position of the particle (x_0) and initial momentum of the particle (p_0) or velocity (v_0).

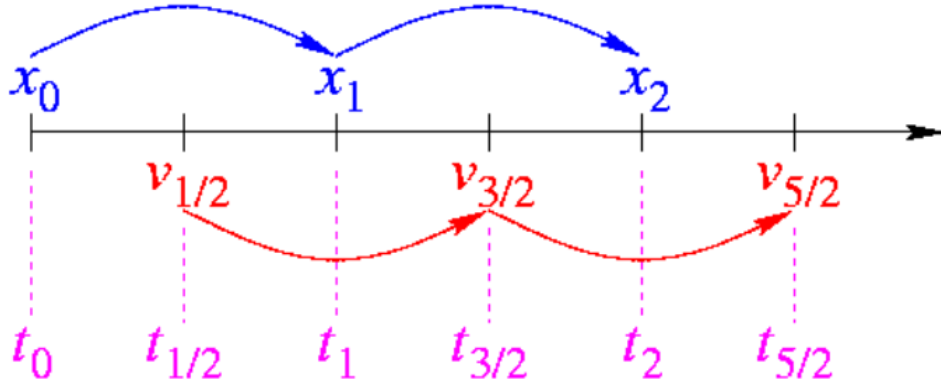


Figure 2.1: Pictorial representation of iteration steps in Leapfrog method

For our SHM problem

$$\frac{dx}{dt} = p(x)/m \text{ and } \frac{dp}{dt} = -kx \quad (2.3)$$

From x_0 and p_0 , the half step of x by Leapfrog method is

$$x_{\frac{1}{2}} = x_0 + \frac{p_0}{m} \frac{\Delta t}{2} \quad (2.4)$$

Now, by Leapfrog method full step on p and x can be calculated for rest of $n = 0$ to $n = N$ by

$$p(n+1) = p_n - kx_{n+\frac{1}{2}}\Delta t \quad (2.5)$$

again,

$$x_{n+\frac{3}{2}} = x_{n+\frac{1}{2}} + \frac{p_{n+1}}{m} \Delta t \quad (2.6)$$

There are two primary strengths to leapfrog integration when applied to mechanics problems. The first is the time-reversibility of the Leapfrog method. One can integrate forward n steps, and then reverse the direction of integration and integrate backwards n steps to arrive at the same starting position. The second strength is its symplectic nature, which implies that it conserves the (slightly modified) energy of dynamical systems. This is especially useful when computing orbital dynamics, as many other integration schemes, such as the (order-4) Runge–Kutta method, do not conserve energy and allow the system to drift substantially over time.

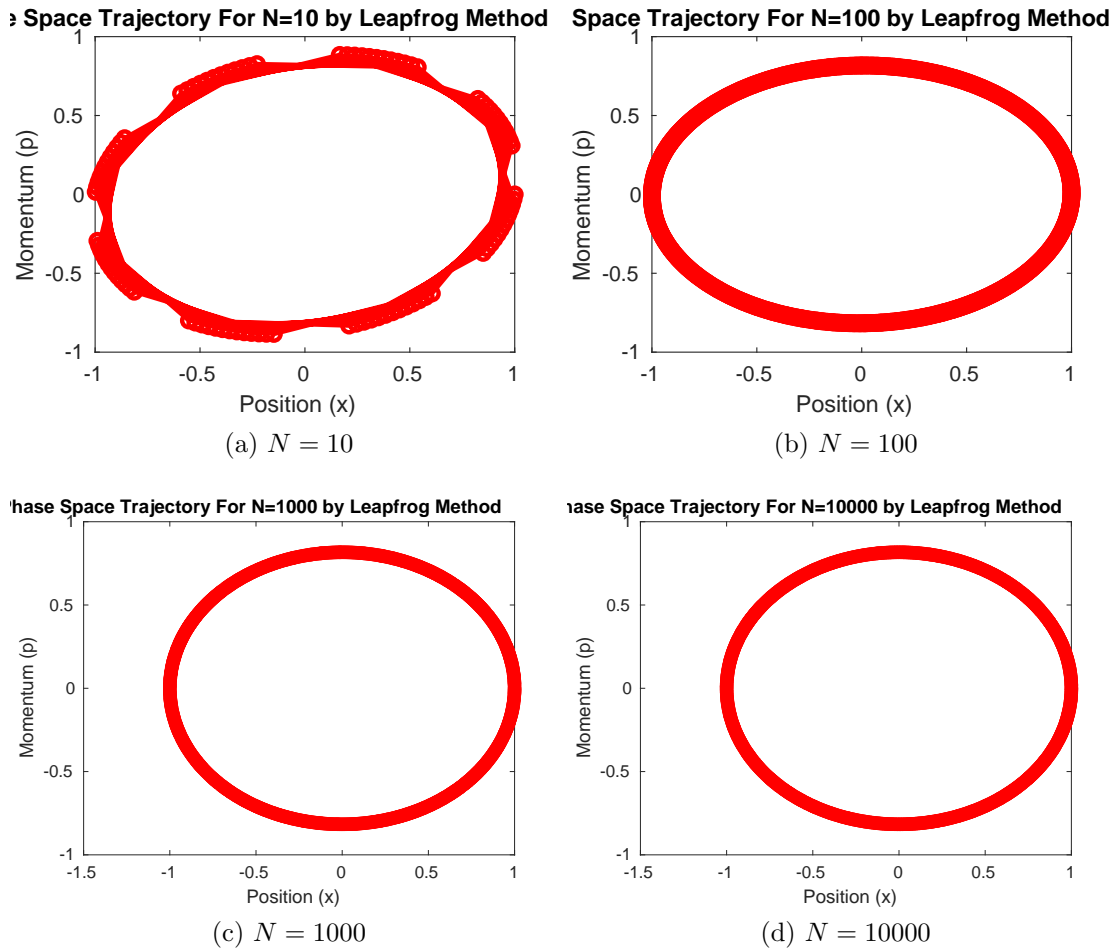


Figure 2.2: Phase space trajectories for different number of steps (N) inside a full time period T (By Leapfrog method)

2.4 Explanation of Plots

In figure 2.2 we plot the phase-space trajectories for different number of steps (N) inside a time period. We can see for $N = 10$ also we get an ellipse (slightly of axis from the analytical solution). The best thing is that like Euler and RK method for small N , like the case of $N = 10$ the solution is not diverging here. This clearly shows why the Leapfrog method is reversible.

In figure 2.3 we plot the $x(t)$ versus t . The solution is stable, unlike the solutions from Euler method and RK method, Leapfrog method gives a stable solution over time. So even for small N the solution is not diverging. That ensures that in leapfrog method the error accumulation is very small.

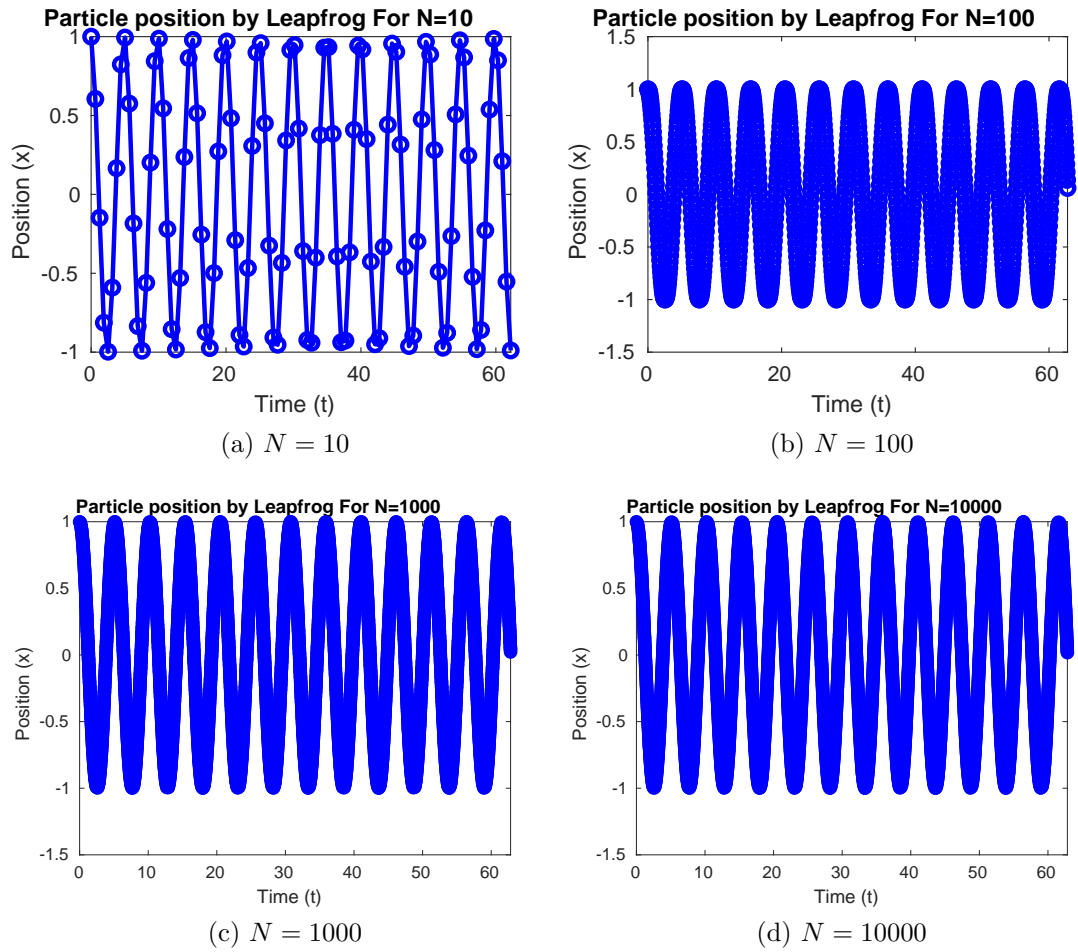


Figure 2.3: Solution of $x(t)$ vs t plot for different number of steps (N) inside a full time period T (By Leapfrog method)

Figure 2.4 shows the constancy of total energy with time. Unlike the Euler method and RK method, here we are not getting a ever growing or ever falling energy pattern. The total energy here oscillates around a constant energy value. The average line of this oscillation is the constant energy value of the system.

2.5 Discussions and Conclusions

As we discussed the error in energy in Leapfrog method is negligible. In figure 2.4 we have plotted relative error ($\varepsilon = \frac{\Delta E}{E}$) with number of steps N in log scale. In figure 2.4 the first plot (plot (a)) shows the negligible amount of energy change for a change in N . The change is so small that when we plot the relative error in Leapfrog method

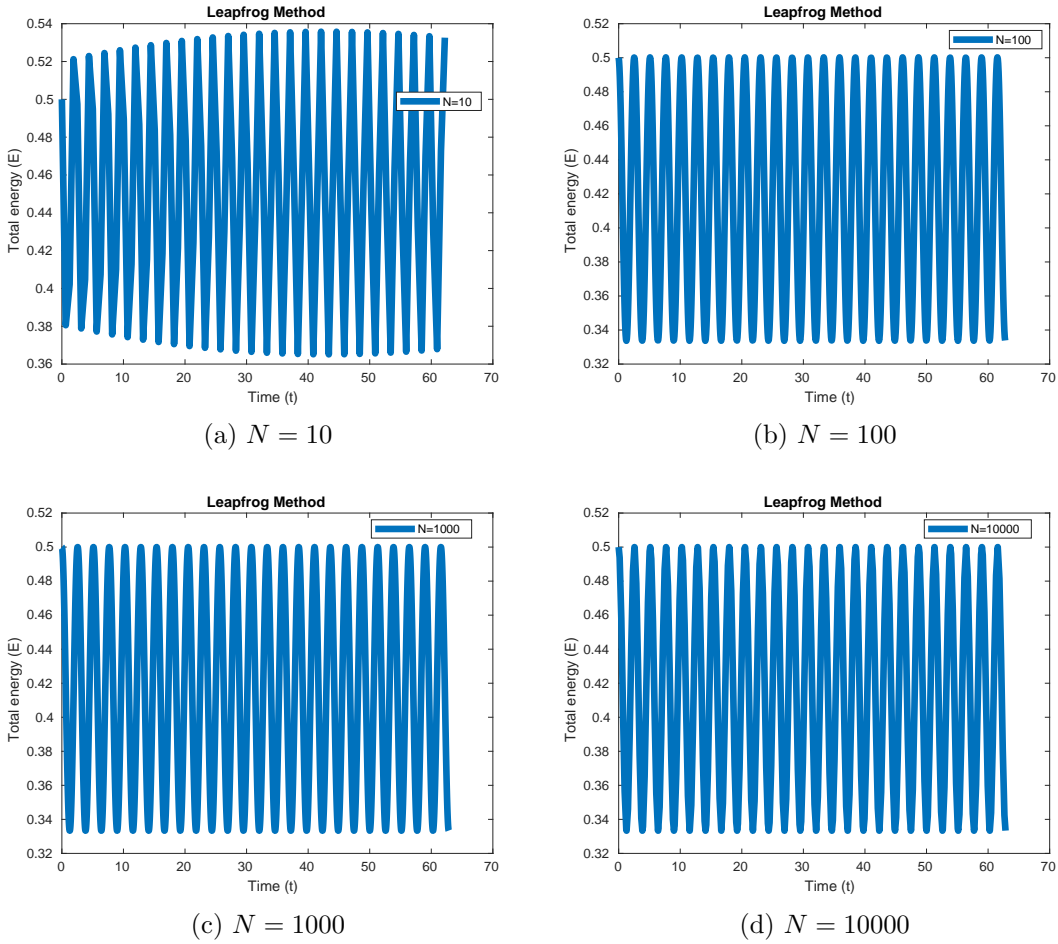
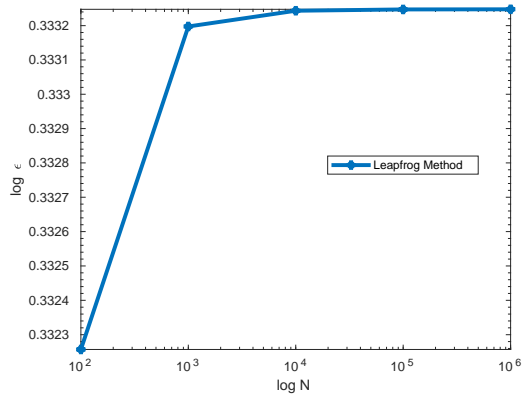


Figure 2.4: Constant energy value of the solution over time (By Leapfrog method). We can see the energy is oscillating around a constant value with very small amplitude.

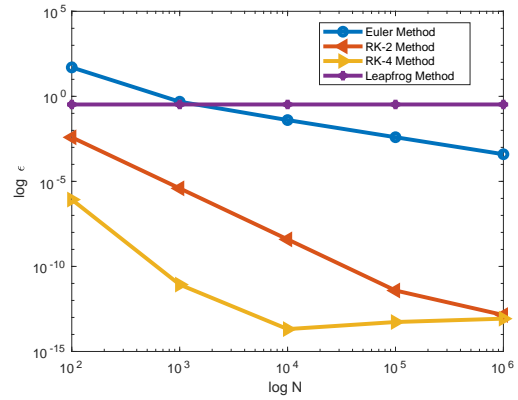
with the relative errors from other methods like Euler, RK-2 and RK-4 (figure 2.4), the Leap frog method form a horizontal line close to $\varepsilon = 0$ in ε vs. N plot. This plot confirms that Leapfrog method is best energy conserving method.

So, whenever in a system we need energy conserving results, Leapfrog method is the best way.

- 1) It is very simple to implement.
- 2) It is first order so computational complexity is less.
- 3) It gives stable solution.
- 4) The error accumulation in each step is negligible.
- 5) The solutions are reversible.



(a) For Leapfrog only



(b) Comparison with other methods

Figure 2.5: ϵ vs N plot in log-log scale for different numerical methods

- 6) The solutions are energy conserving.
- 7) For small number of steps N the solution is not diverging.

Chapter 3

Solution of Poisson's Equation using Finite Difference Method

3.1 Aim

To discuss the Finite Difference Method (FDM) and solve Poisson's equation using FDM.

3.2 Introduction

Our goal is to solve Poisson equation. In previous assignments we learnt how to solve Poisson equation using Fourier method. In this assignment we will solve Poisson equation by more direct approach, Finite difference method.

3.3 Brief Theory

We want to solve

$$\nabla^2 \phi = 4\pi G\rho \quad (3.1)$$

where ρ is given and we want to solve for ϕ . In 1D the Poisson equation is

$$\frac{d^2 \phi}{dx^2} = 4\pi G\rho \quad (3.2)$$

Now, by Taylor series expansion we have

$$\phi(x+h) = \phi(x) + h\phi'(x) + \frac{h^2}{2}\phi''(x) + \dots \quad (3.3)$$

$$\phi(x - h) = \phi(x) - h \phi'(x) + \frac{h^2}{2} \phi''(x) - \dots \quad (3.4)$$

By eq (3.3) – eq (3.4) we have

$$\phi'(x) = \frac{\phi(x + h) - \phi(x - h)}{2h} + \frac{\mathcal{O}(h^3)}{h} \quad (3.5)$$

and by eq (3.3) + eq (3.4) we have

$$\phi''(x) = \frac{\phi(x + h) + \phi(x - h) - 2\phi(x)}{h^2} + \frac{\mathcal{O}(h^3)}{h^2} \quad (3.6)$$

Eq. 3.5 and eq. 3.6 shows the discrete version of first and second derivative of a function respectively. In the discrete form eq 3.2 can be written as

$$\frac{\phi(x + h) + \phi(x - h) - 2\phi(x)}{h^2} = 4\pi G\rho(x) + \frac{\mathcal{O}(h^3)}{h^2} \quad (3.7)$$

In discrete space (computational space) x is replaced by discrete integer a .

$$\boxed{\frac{\phi_{a+1} + \phi_{a-1} - 2\phi_a}{L^2} = 4\pi G\rho_a} \quad (3.8)$$

neglecting higher order terms, L is the grid spacing.

3.4 Simulation Parameters

We done the simulation for a 2D grid, the parameters are:

- 1) square grid side length = 100
- 2) grid spacing $L = 1$
- 3) The value of potential ϕ at boundaries of the square grid is assumed to be zero (As with distance the potential value falls down, and for infinite distance it is zero. However we can not work with infinity, so it is a good approximation to set potential values zero at boundaries of the finite square grid over that we are simulating).

3.5 Potential Plots

Figure 3.1 to figure 3.4 shows potential solutions for different source mass configurations. (For getting a clear plot I just reverse the sign of the potential before plotting).

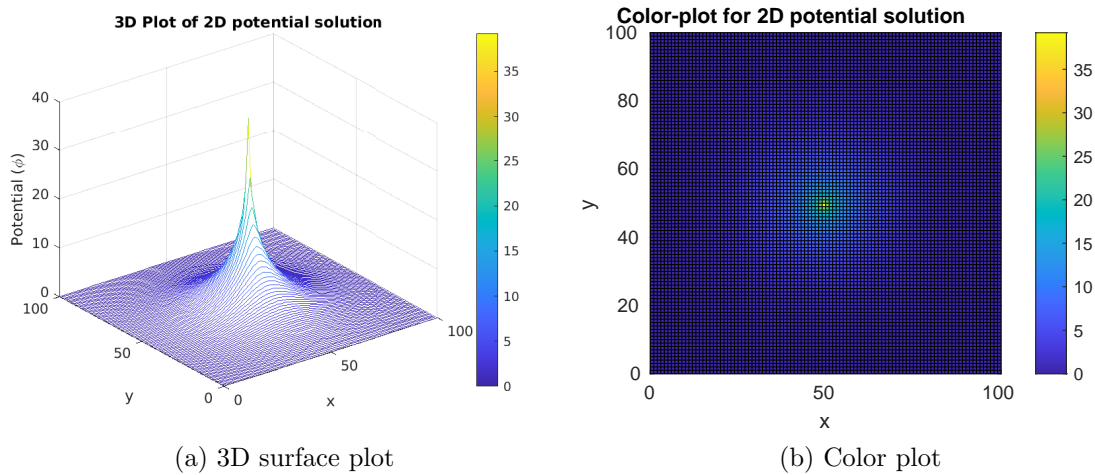


Figure 3.1: Potential (ϕ) plot for a point mass at the centre (50,50) of 2D grid (100 \times 100)

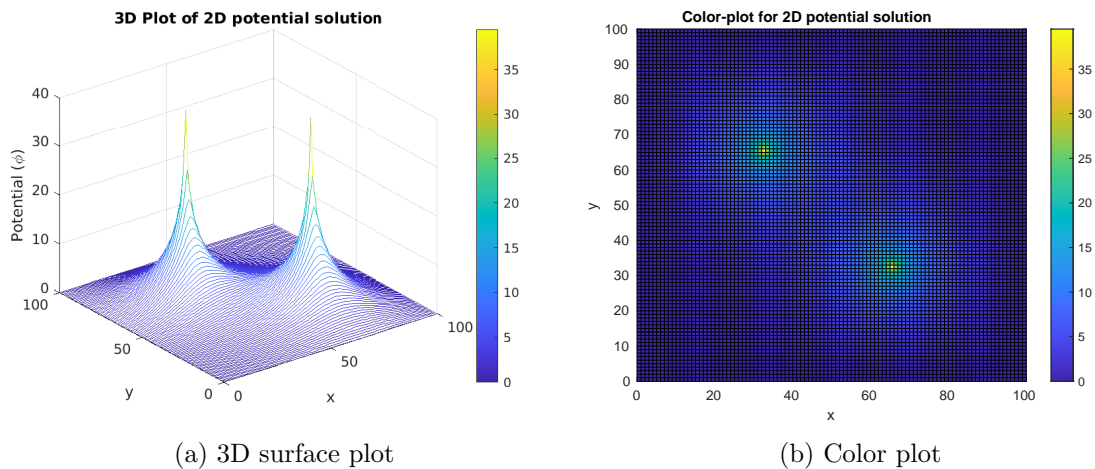


Figure 3.2: Potential (ϕ) plot for two point masses at (33,66) and (66,33) of a (100 \times 100) 2D grid

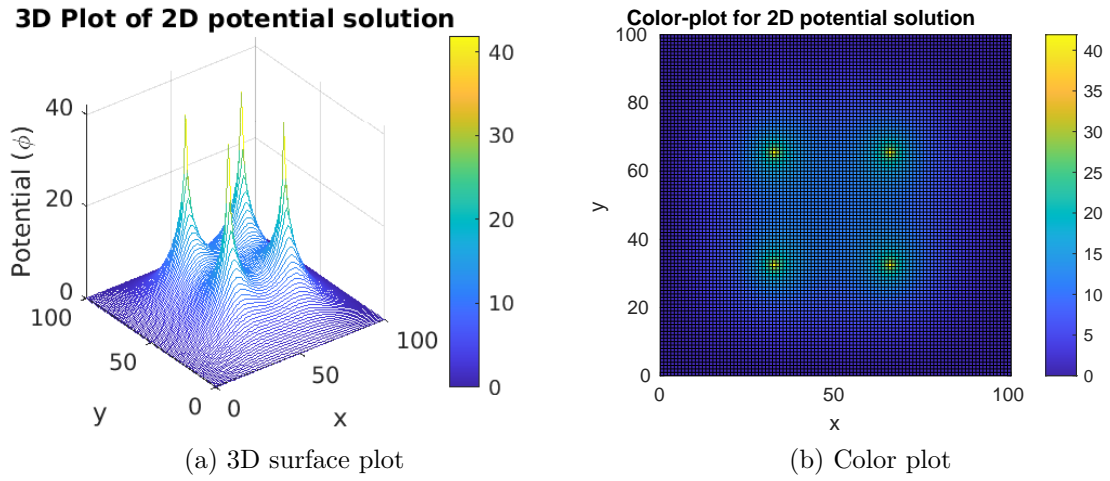


Figure 3.3: Potential (ϕ) plot for four point masses at $(33, 66)$, $(33, 33)$, $(66, 33)$ and $(66, 66)$ of a (100×100) 2D grid

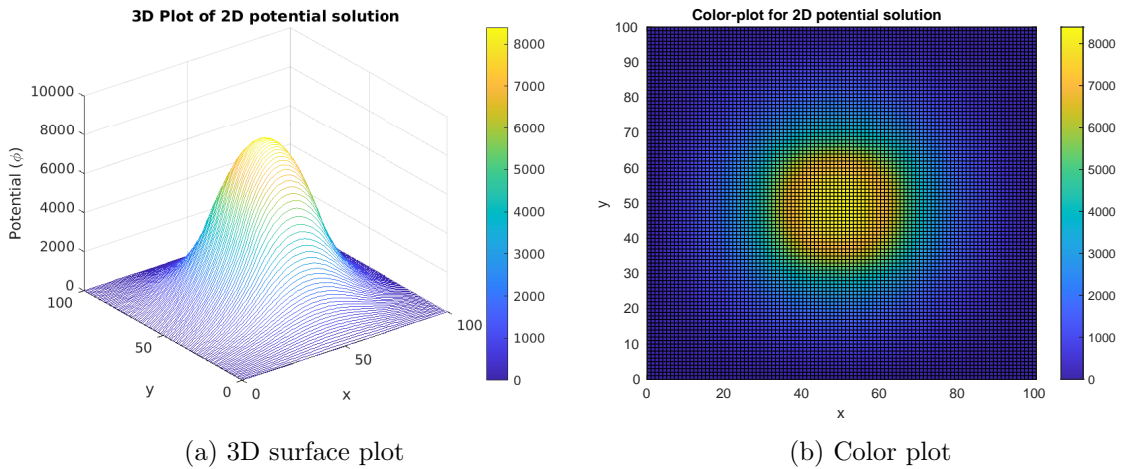


Figure 3.4: Potential (ϕ) plot for a square 2D uniform bulk mass distributed between $x = 33$, $x = 66$, $y = 33$ and $y = 66$ of a (100×100) 2D grid

Chapter 4

Fourier Method Solution of Poisson's Equation

4.1 Aim

To find the potential-field and acceleration-field created by a known mass density distribution (ρ) for 1D system by Fourier transform and inverse Fourier transform method.

4.2 Introduction

We can write any function in Fourier series expansion, as the terms in Fourier series forms a complete basis set. Same is true for Fourier transform. Fourier transform forms a complete continuous basis to expand any function.

We want to solve the potential and finally acceleration field created by a mass density distribution (ρ). So, the source mass distribution is ρ , which is known as function of distance.

We cannot deal with continuous variables in computation. The distance x is just a number a in discrete system. So we have ρ_a . By discrete Fourier transform of this we have

$$\tilde{\rho}_n = \frac{1}{N} \sum_{a=0}^{N-1} \rho_a \exp \left[-\frac{2\pi i n a}{N} \right] \quad (4.1)$$

From this mass density in Fourier space we can calculate the potential in Fourier space via the Formula derived in the class:

$$\tilde{\phi}_n = -\frac{(4\pi G)\tilde{\rho}_n L^2}{4 \sin^2 \frac{\pi n}{N}} \quad \text{for } n > 0 \quad (4.2)$$

The acceleration-field in Fourier space can be calculated using the formula:

$$\tilde{A}_n = -i \sin\left(\frac{2\pi n}{N}\right) \frac{\tilde{\phi}_n}{L} \quad (4.3)$$

Now, we have $\tilde{\phi}_n$ and \tilde{A}_n , so, we can just take inverse Fourier transform to calculate our require potential field ϕ_a and acceleration field A_a in real space:

$$\phi_a = \sum_{n=0}^{N-1} \tilde{\phi}_n \exp\left[\frac{2\pi i n a}{N}\right] \quad (4.4)$$

and,

$$A_a = \sum_{n=0}^{N-1} \tilde{A}_n \exp\left[\frac{2\pi i n a}{N}\right] \quad (4.5)$$

4.3 Problem Parameters

In this assignment we take a 1D grid of grid size $N = 128$. We work with three types of mass density ρ_a .

4.4 Explanation of Plots

In figure 4.1 and figure 4.2 we have a point mass (source) at $a = 64$. For this mass configuration these figure shows the plots for all different parameters in real and Fourier space. We plotted real and imaginary parts separately for all complex parameters.

In figure 4.3 and figure 4.4 the source is two point masses situated at $a = 40$ and $a = 80$.

In figure 4.5 and figure 4.6 the source is three point masses situated at $a = 20$, $a = 40$ and $a = 60$.

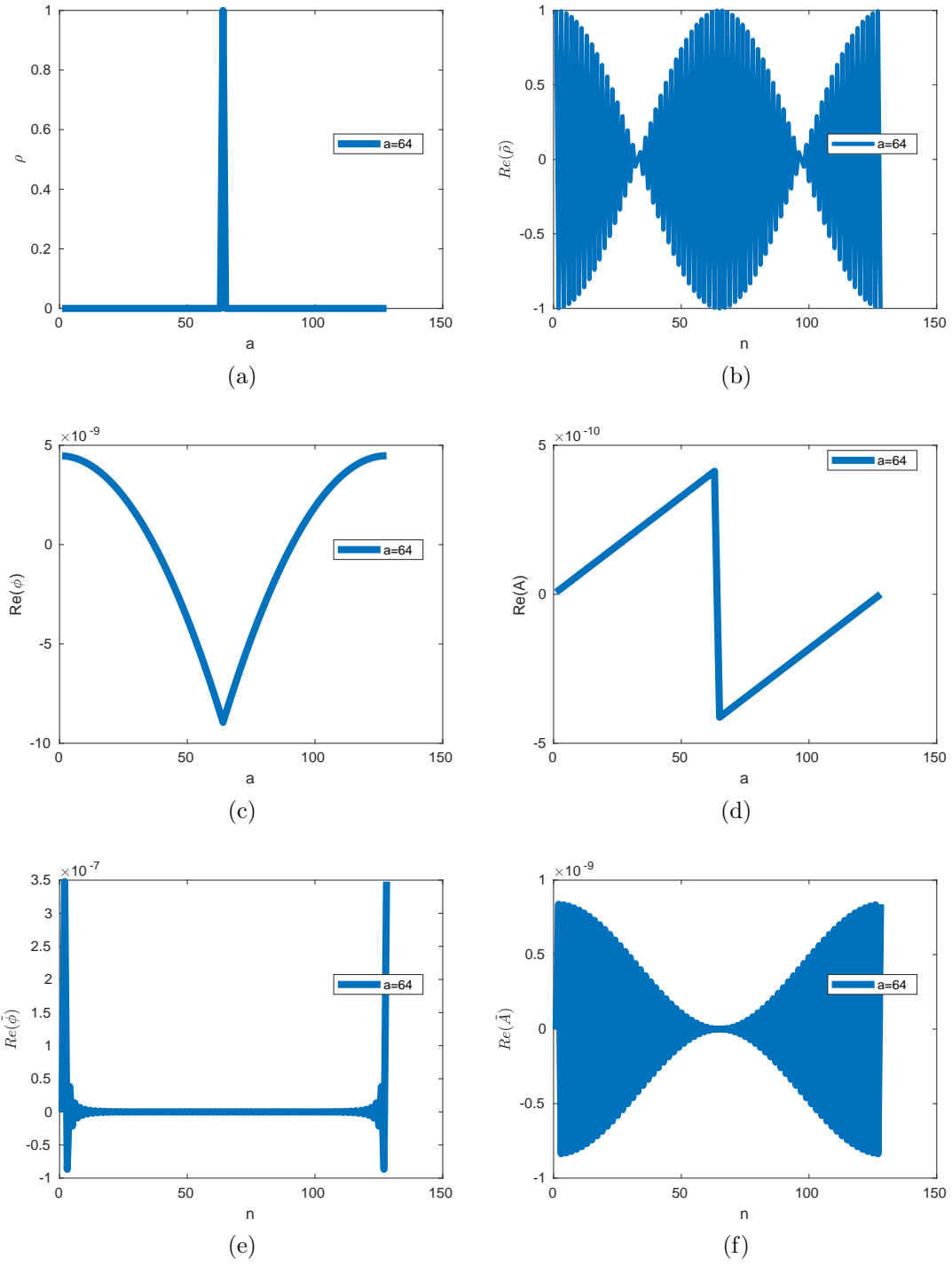


Figure 4.1: Real parts of all different complex parameters (a point mass at $a = 64$ is the source mass)

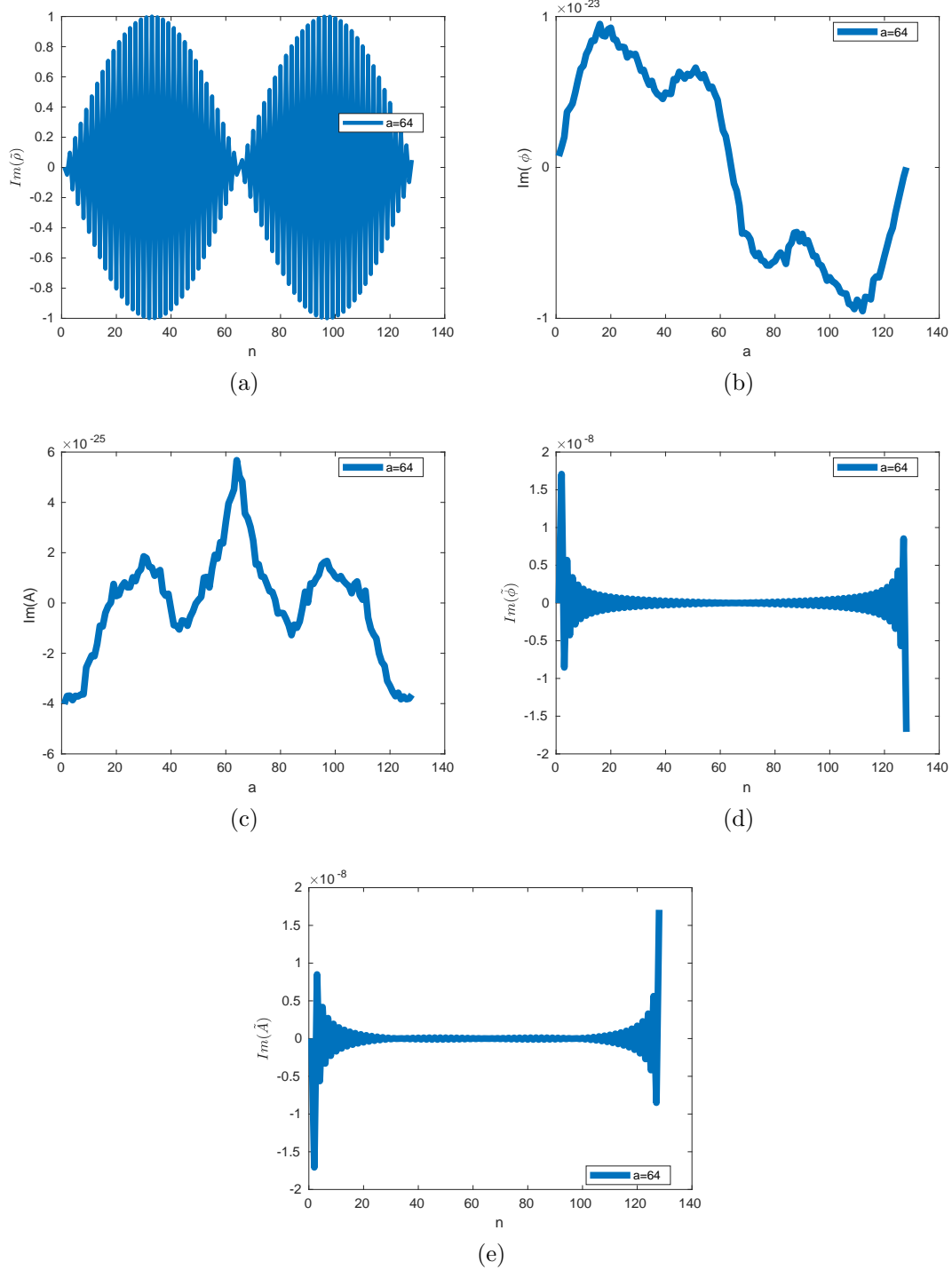
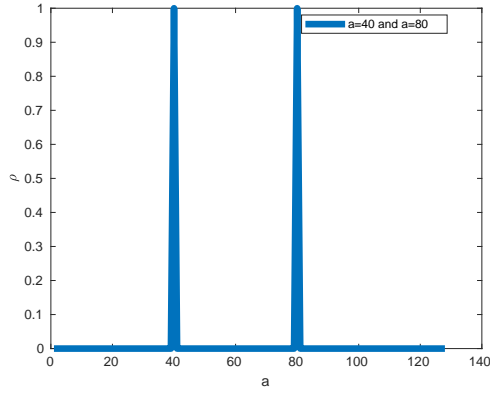
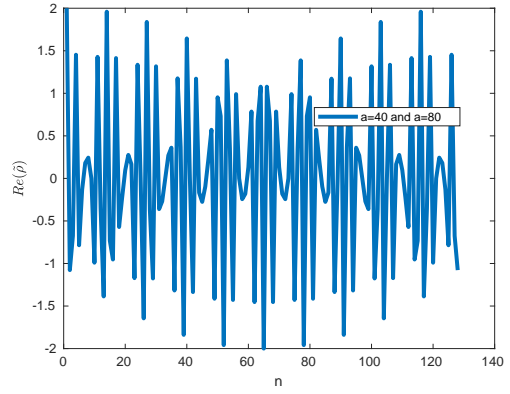


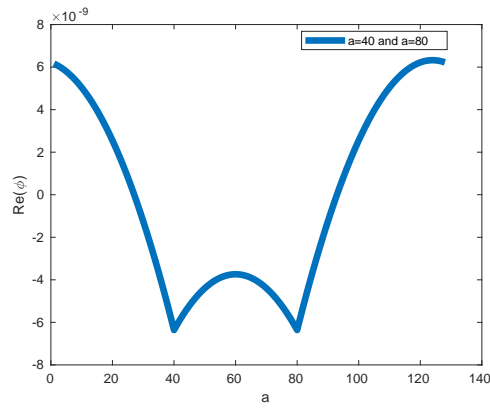
Figure 4.2: Imaginary parts of all different complex parameters (a point mass at $a = 64$ is the source mass)



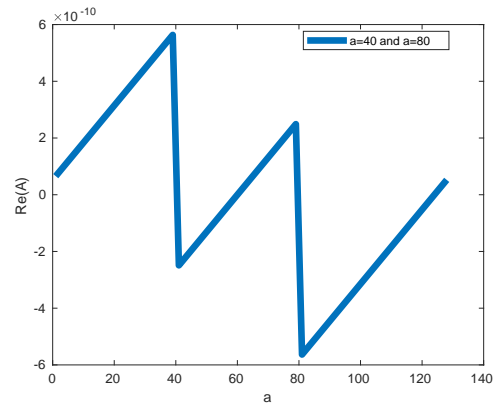
(a)



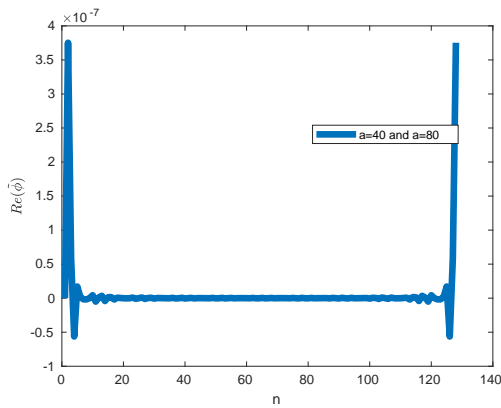
(b)



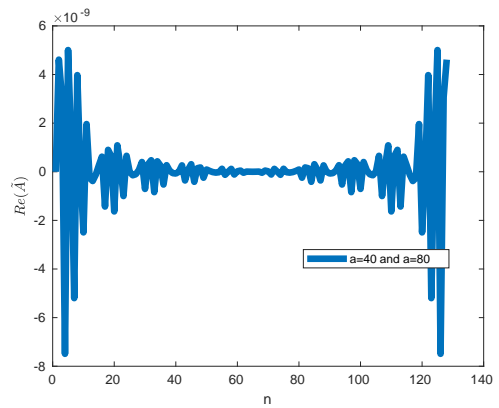
(c)



(d)



(e)



(f)

Figure 4.3: Real parts of all different complex parameters (two point masses at $a = 40$ and $a = 80$ are the source distribution)

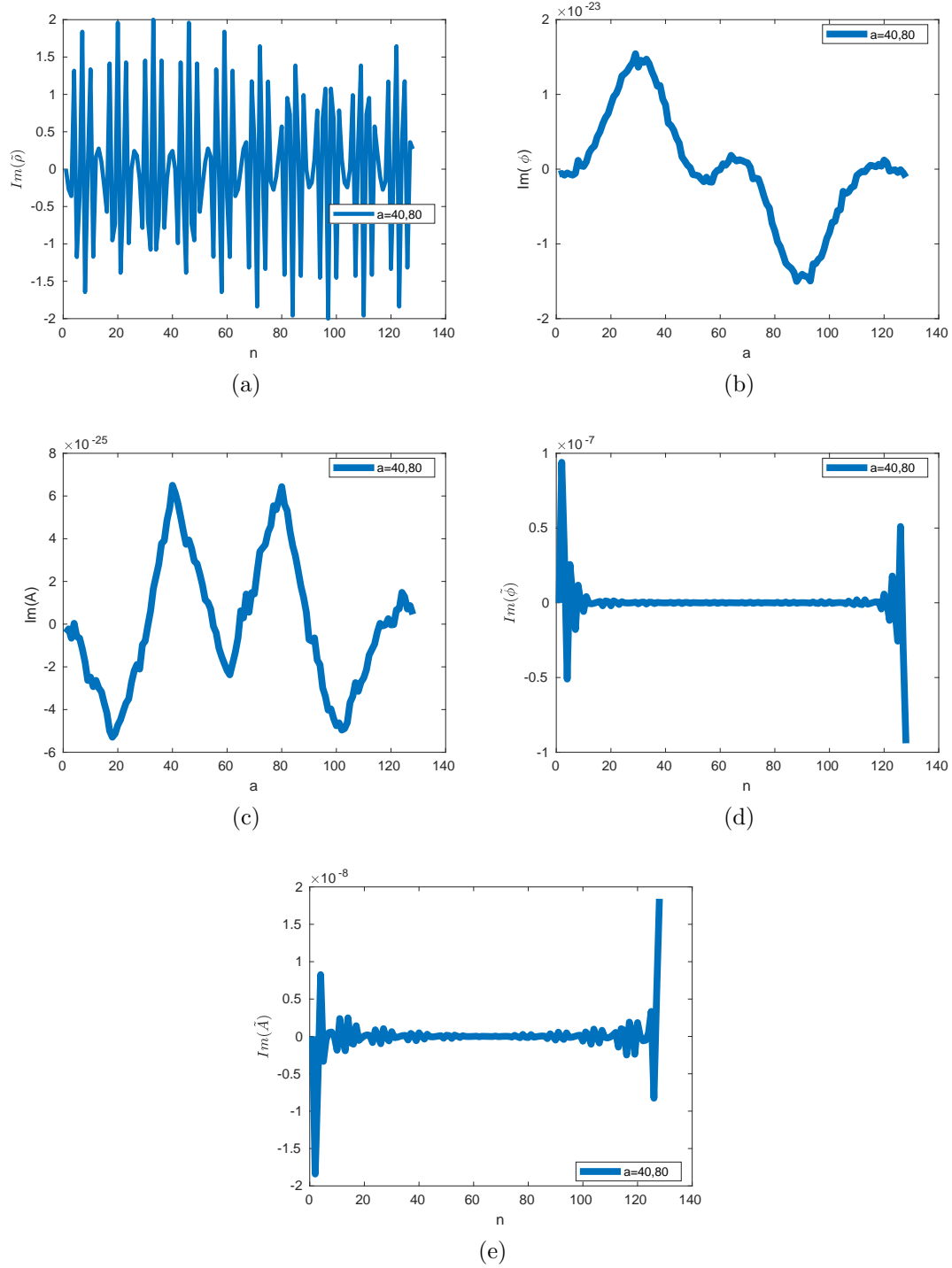
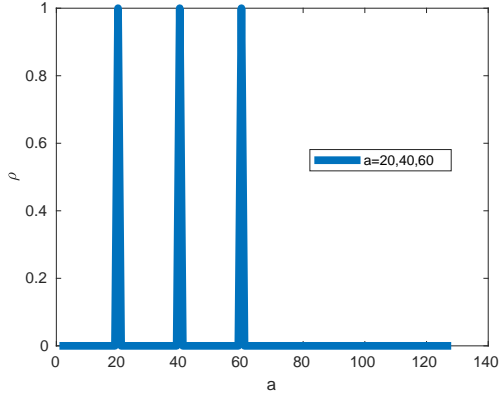
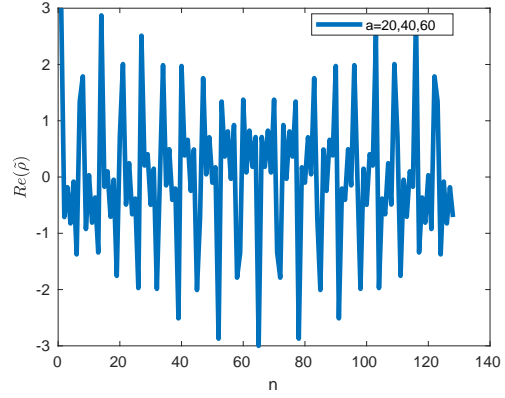


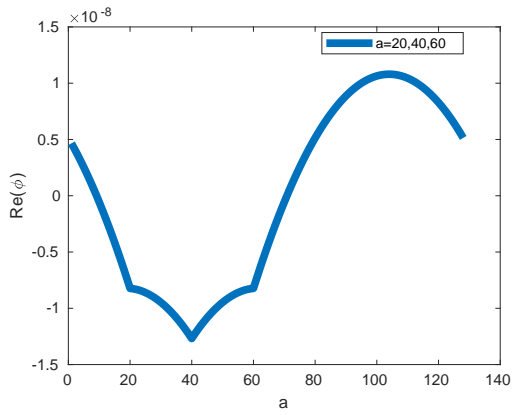
Figure 4.4: Imaginary parts of all different complex parameters (two point masses at $a = 40$ and $a = 80$ are the source distribution)



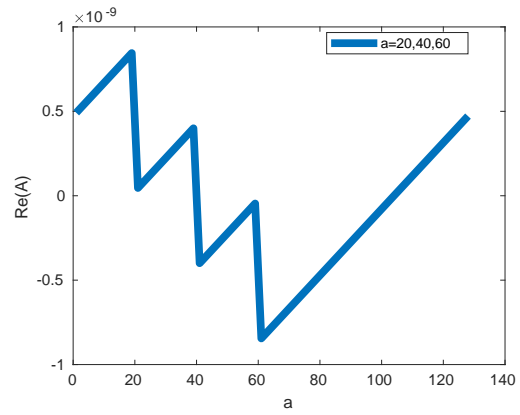
(a)



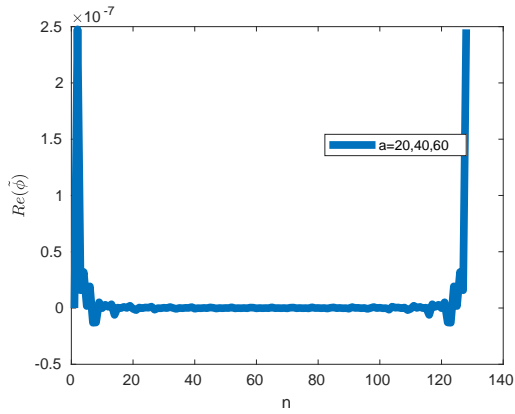
(b)



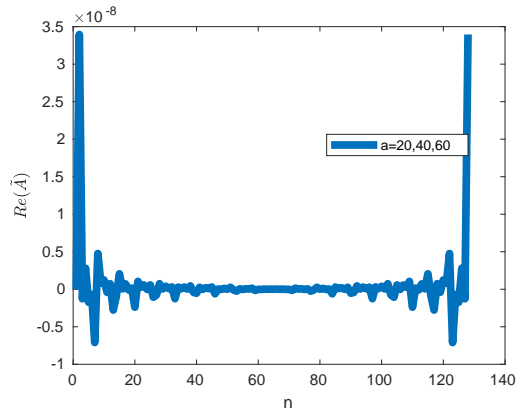
(c)



(d)



(e)



(f)

Figure 4.5: Real parts of all different complex parameters (three point masses at $a = 20$, $a = 40$ and $a = 60$ are the source distribution)

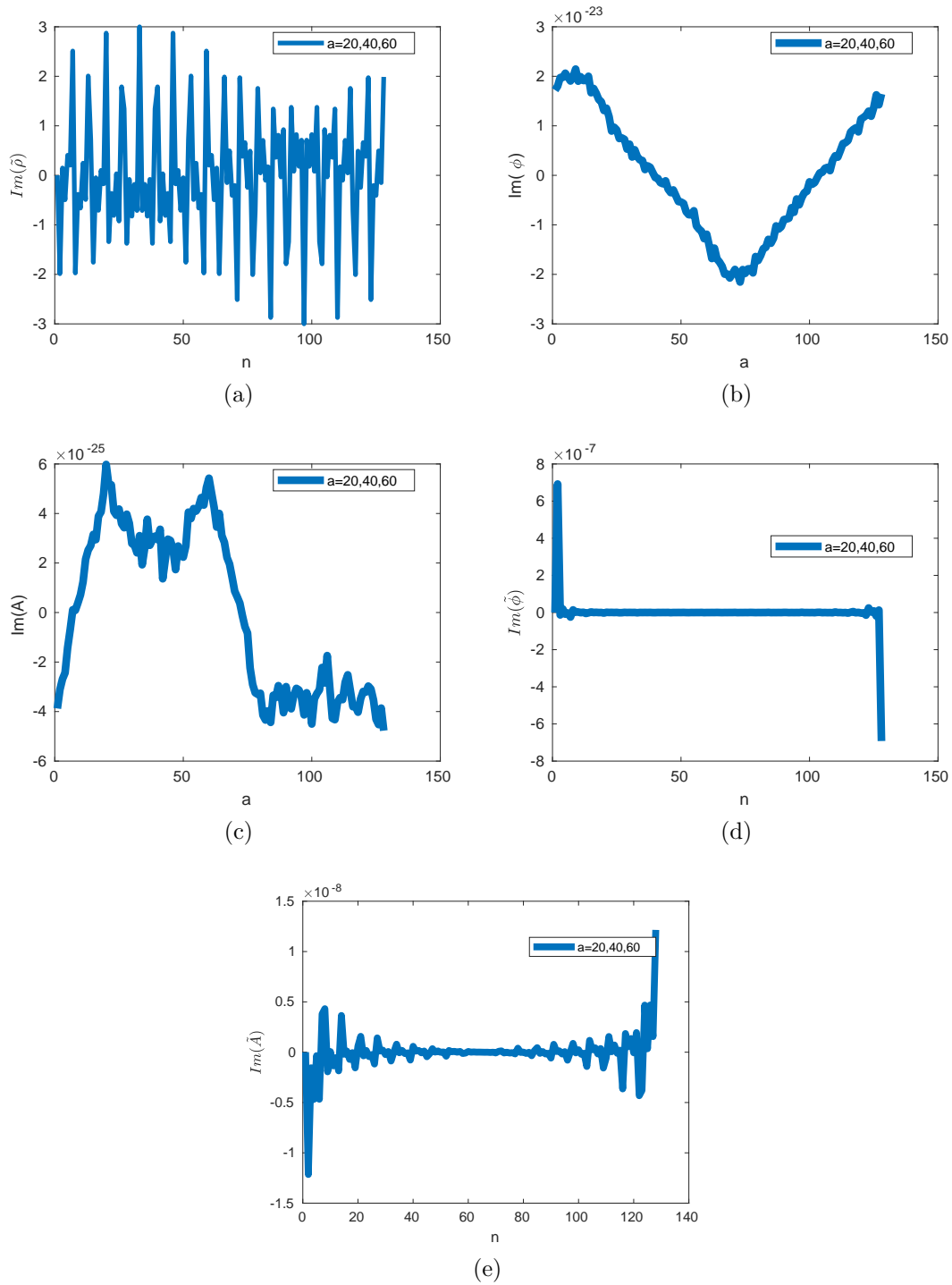


Figure 4.6: Imaginary parts of all different complex parameters (three point masses at $a = 20$, $a = 40$ and $a = 60$ are the source distribution)

Chapter 5

Solution of Poisson's Equation by CIC Method

5.1 Aim

To find the acceleration value at test particle position, where in generally test particle may not be situated on a grid position.

5.2 Introduction

In Assignment-4 we solved the acceleration and potential field for a given mass density. However the acceleration and potential field that we calculated there is on the grid. The density of particles also was distributed on the grid points only. In real physical problem the source particle and test particle positions may not be always on a grid point. In generally it can be anywhere between the grid points.

In that case we have to use Cloud in Cell (CIC) method.

5.3 Brief Theory

If the position for any source particle between two grid points is x then according to CIC method the mass of the particle will distribute among the grid points. The mass distribution will be weighted average. The closer a mass particle to a grid point, more weight will be given for that grid point.

For a 1D case if the source particle position is x and it is situated between the grid points $a = floor$ and $a = ceil$. If the mass of the particle is m then

$$w_1 = 1 - |x - floor| \text{ and } w_2 = 1 - |ceil - x| \quad (5.1)$$

and,

$$\rho_{floor} = w_1 \times m \text{ and } \rho_{ceil} = w_2 \times m \quad (5.2)$$

Now, as we have density of mass on the grid the calculation of potential field and acceleration on the grid is as the previous assignment (Assignment-4).

If the test particle is at x_{test} and situated between the grid points $a = ft$ and $a = ct$ then acceleration at x_{test} is

$$A(x_{test}) = w_1 \times A_{ft} + w_2 \times A_{ct} \quad (5.3)$$

where,

$$w_1 = 1 - |x - ft| \text{ and } w_2 = 1 - |ct - x| \quad (5.4)$$

5.4 Simulation Parameters

We simulate for a 1D grid of $L = 128$.

The source is an unit point mass at $x = 64.4$

The test particle is an unit point mass at $x_{test} = 10.8$

5.5 Results and Plots

The value of the acceleration at the test particle position ($x_{test} = 10.8$) is $A(x_{test}) = 6.814577850552632 \times 10^{-11} \text{ N/kg}$

For this system we plot the real and imaginary solutions of different real and Fourier space parameters in the figure 5.1 (real parts of the solutions) and figure 5.2 (imaginary parts of the solutions).

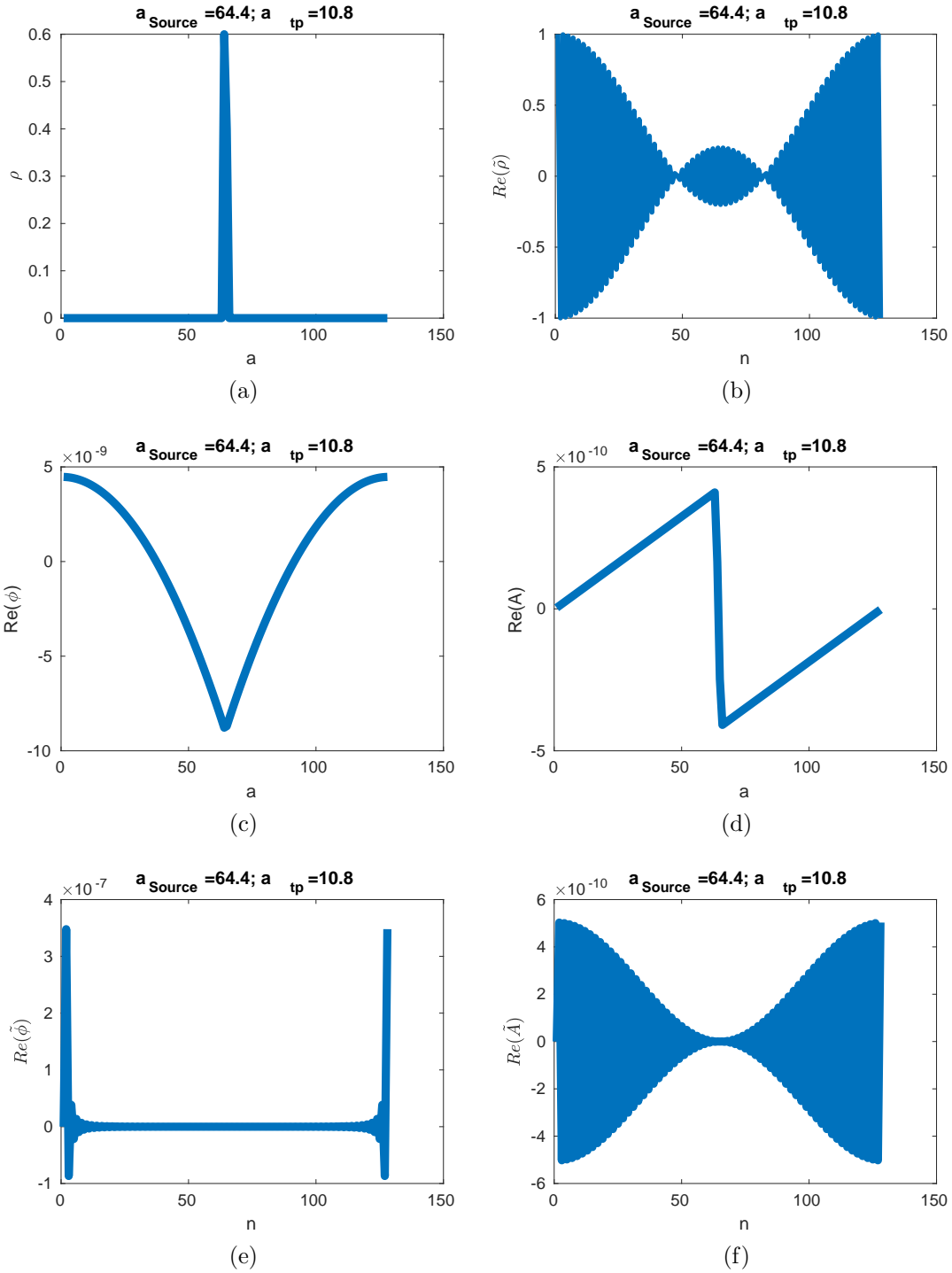


Figure 5.1: Real parts of all different complex parameters (The source particle is at $x = 64.4$ and test particle is at $x_{\text{test}} = 10.8$)

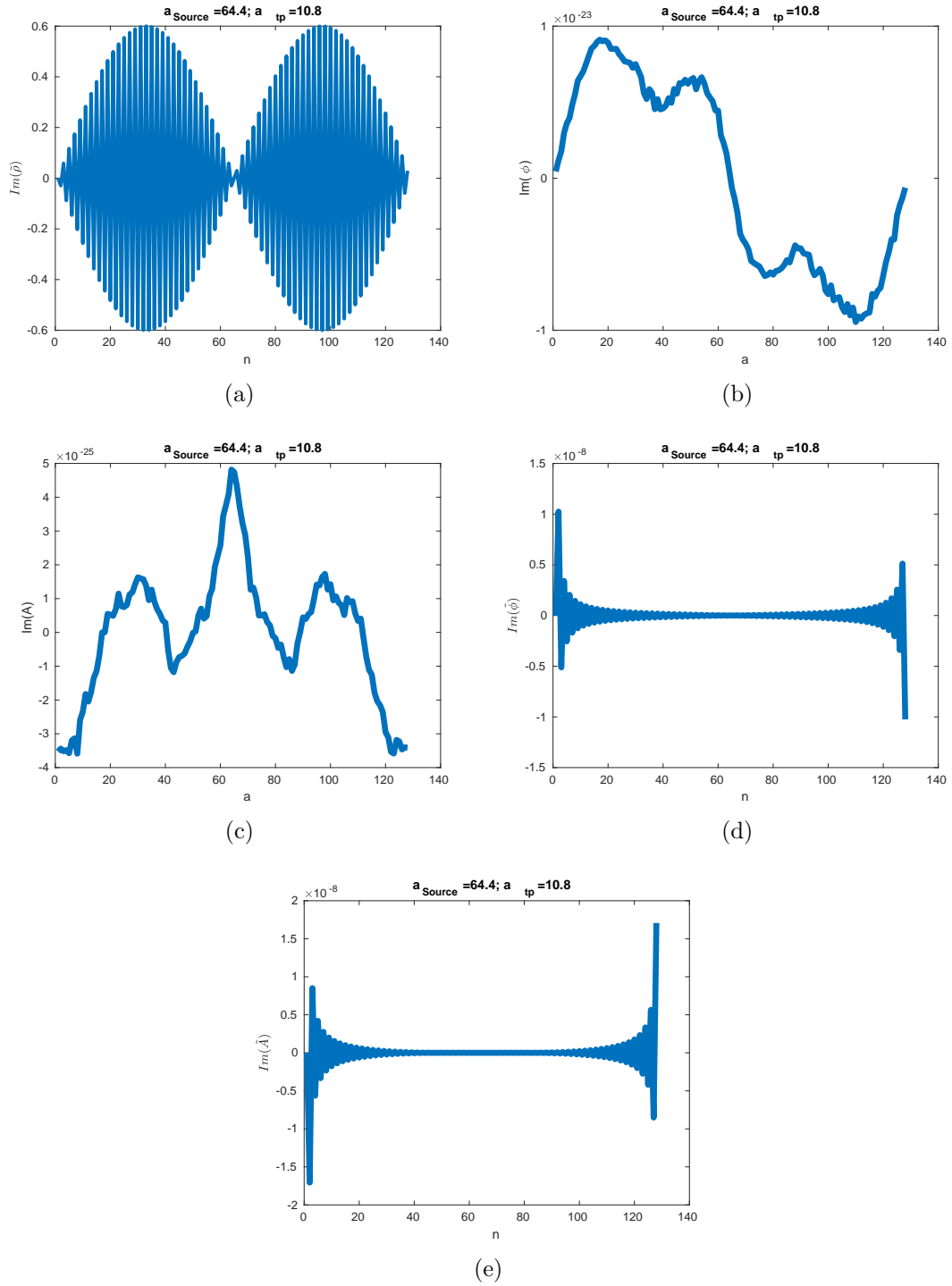


Figure 5.2: Imaginary parts of all different complex parameters (The source particle is at $x = 64.4$ and test particle is at $x_{\text{test}} = 10.8$)

Chapter 6

Simulation of 1D Self-Gravitating System

6.1 Aim

To simulate a 1D distribution of particle under the influence of its own gravity. To draw the phase space snapshots over time.

6.2 Introduction

After doing all the previous assignments we now know how to solve differential equation, we know that by Leapfrog method the solution is energy conserving. From assignment-4 we know how to solve Poisson's equation using Fourier method. From assignment-5 we know how to even solve for acceleration and potential when the test and source particles are not on grid (by CIC method). Now finally we are going to address our goal, to solve a self gravitating system. In this assignment we solve the 1D self gravtating system.

6.3 Brief Theory

We normalize the time and space using appropriate scaling parameters. We normalize time using $t_g = \frac{a}{\sqrt{G\rho}}$. This t_g is the gravitational time scale, which is the time taken by a uniformly distributed spherical body to collapse. The length x is normalized using the grid spacing L as a scaling length.

So, dimensionless $X = x/L$ and dimensionless $T = t/t_g$

The Hamilton's equation in dimensionless form is

$$\frac{dX}{dT} = \frac{t_g P}{Lm} \quad \text{and} \quad \frac{dP}{dT} = \frac{t_g^2 f}{Lm} = F \quad (\text{dimensionless force}) \quad (6.1)$$

The form of dimensionless force F can be calculated as

$$F = 4\pi \left[-\nabla_x \cdot (\nabla_x^{-2}) \frac{\rho}{\bar{\rho}} \right] \quad (6.2)$$

$\bar{\rho} = 1$ for our simulation, but ρ will evolve as the system evolve.

6.4 Simulation Parameters

Simulation parameters are:

$L = 100$; total space in 1D

$dx = 1$; length of each segment

$N = S/dx$; number of grid points

$T = 100$; total run time

$dt = 0.1$; time step

All the variables are normalized in this simulation.

6.5 Explanation of plots

All the plots in figure 6.1 to figure 6.4 are the phase space snapshots for time $t = 10$ to $t = 800$ with an interval of $t = 10$. We start with particles uniformly distributed over a 1D line with zero momentum. As time pass particles will get momentum due to gravitational attraction and try to collapse (cluster) at the centre. We use periodic boundary condition here.

6.6 Video of the simulation

A video of the simulation done in this assignment can be found in this link <https://youtu.be/tzBqdSGEpTQ>. However with this assignment PDF file the video is also attached.

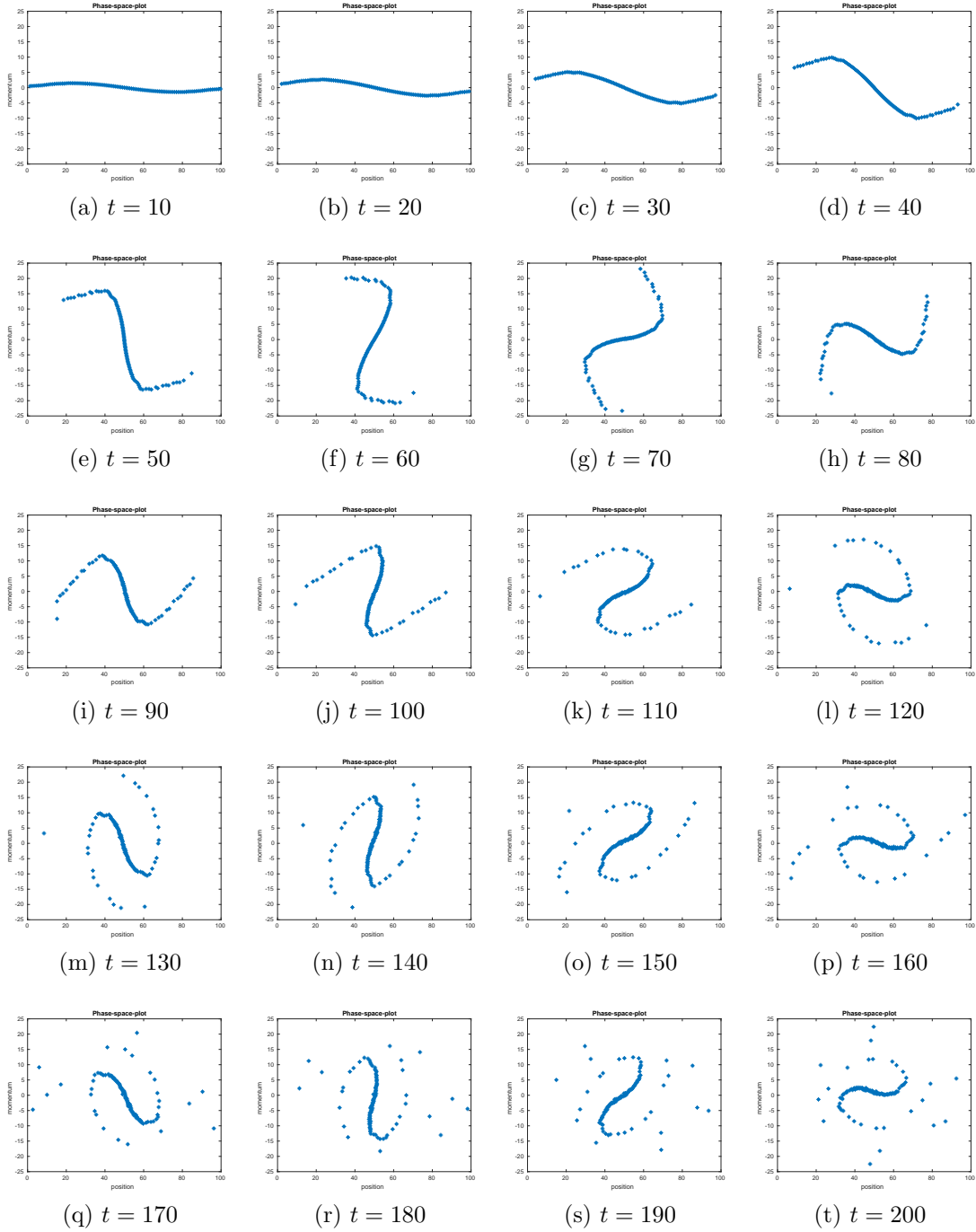


Figure 6.1: Phase Space snapshots for $t = 10$ to $t = 200$ with time separation of 10

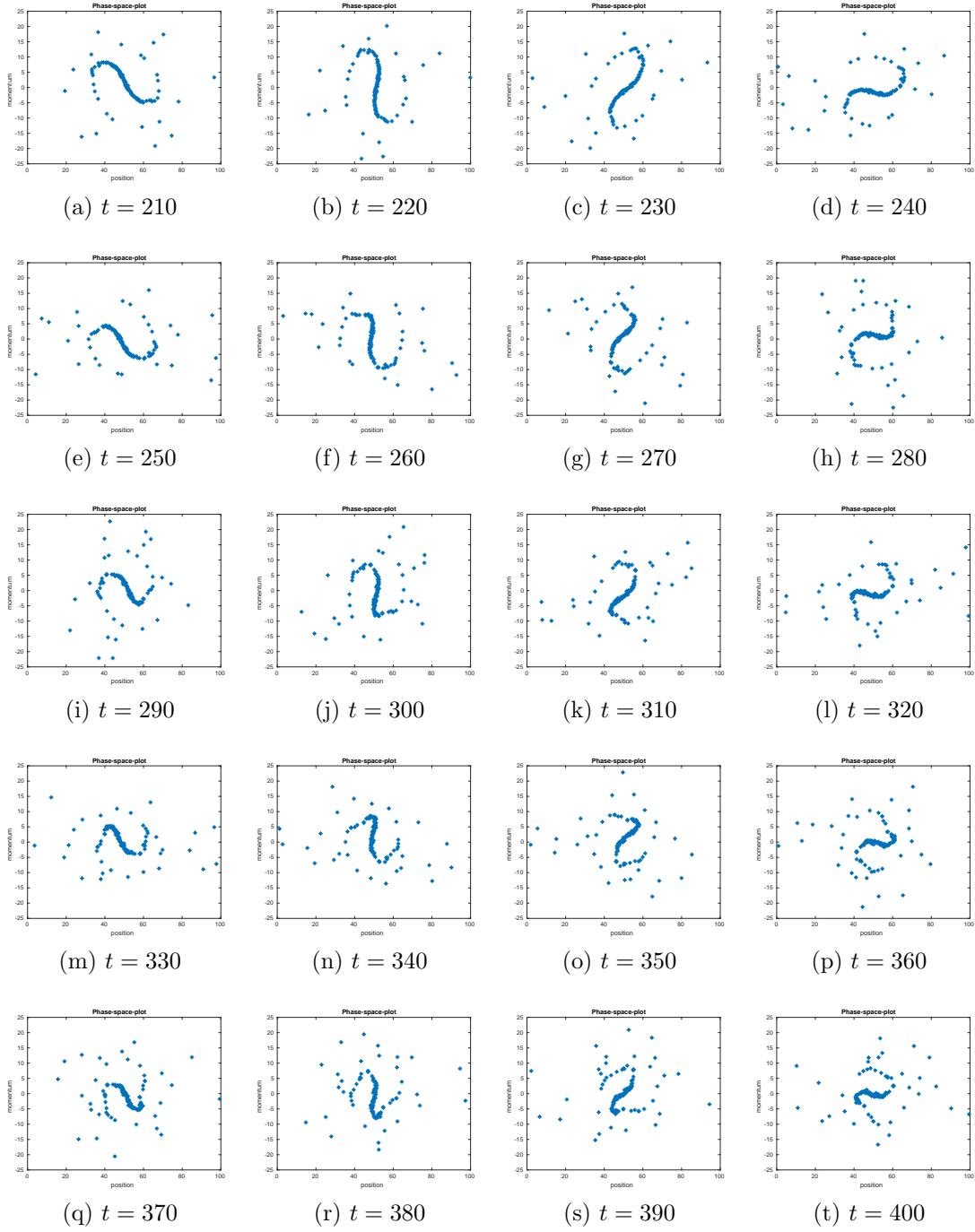


Figure 6.2: Phase Space snapshots for $t = 210$ to $t = 400$ with time separation of 10

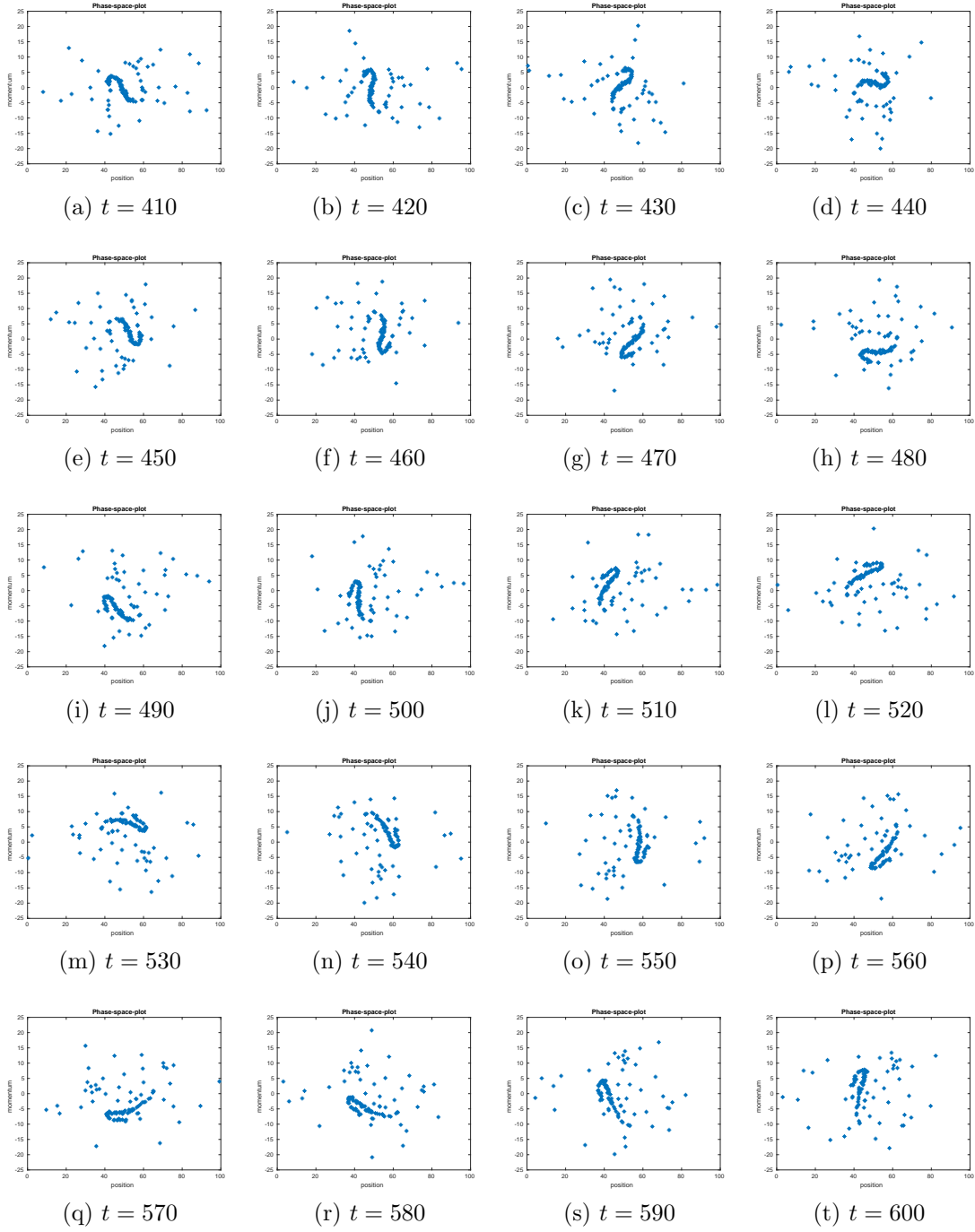


Figure 6.3: Phase Space snapshots for $t = 410$ to $t = 600$ with time separation of 10

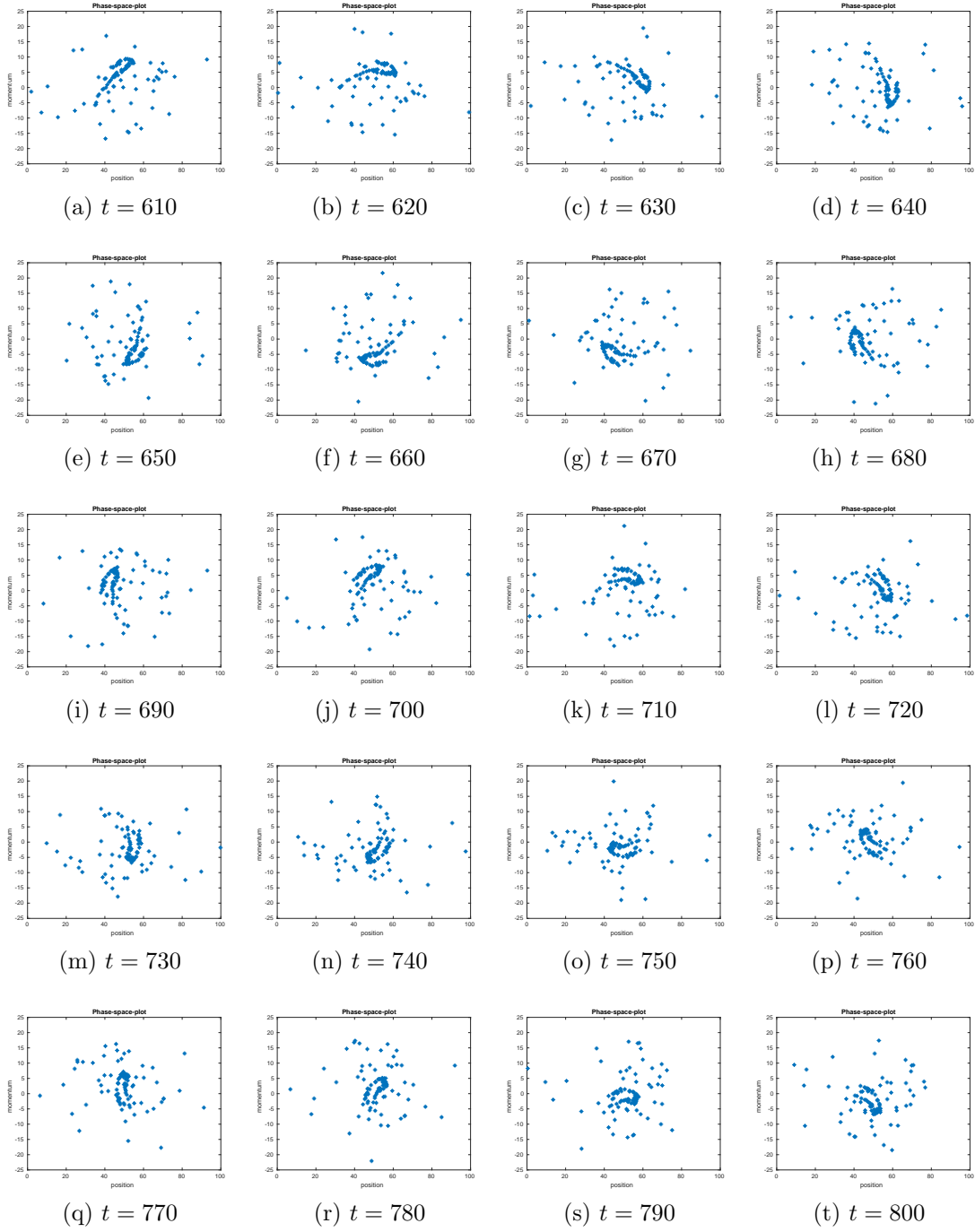


Figure 6.4: Phase Space snapshots for $t = 610$ to $t = 800$ with time separation of 10

Bibliography

- Anastassi, Z. & Simos, T. (2005), ‘An optimized runge–kutta method for the solution of orbital problems’, *Journal of Computational and Applied Mathematics* **175**(1), 1–9.
- Atkinson, K. (1985), ‘The numerical evaluation of particular solutions for poisson’s equation’.
- Bhat, P., Curless, B., Cohen, M. & Zitnick, C. L. (2008), Fourier analysis of the 2d screened poisson equation for gradient domain problems, *in* ‘European Conference on Computer Vision’, Springer, pp. 114–128.
- Butcher, J. C. (1976), ‘On the implementation of implicit runge-kutta methods’, *BIT Numerical Mathematics* **16**(3), 237–240.
- Cash, J. R. & Karp, A. H. (1990), ‘A variable order runge-kutta method for initial value problems with rapidly varying right-hand sides’, *ACM Transactions on Mathematical Software (TOMS)* **16**(3), 201–222.
- Gel’fand, I. M. & Dikii, L. A. (1979), ‘Integrable nonlinear equations and the liouville theorem’, *Functional Analysis and its Applications* **13**(1), 6–15.
- Ghosh, T., Pramanick, S., Sarkar, S., Dey, A. & Chandra, S. (2020), ‘Dynamical properties and effects of quantum diffraction on the propagation of e-a-solitary waves in three-component fermi plasma’, *arXiv:2012.13616v1* p. 8.
- Greiner, A., Strittmatter, W. & Honerkamp, J. (1988), ‘Numerical integration of stochastic differential equations’, *Journal of Statistical Physics* **51**(1-2), 95–108.
- Hahn, G. (1991), ‘A modified euler method for dynamic analyses’, *International Journal for Numerical Methods in Engineering* **32**(5), 943–955.

- Iserles, A. (1986), ‘Generalized leapfrog methods’, *IMA Journal of Numerical Analysis* **6**(4), 381–392.
- Jordan, T. F. (2004), ‘Steppingstones in hamiltonian dynamics’, *American journal of physics* **72**(8), 1095–1099.
- Liu, T., Zhao, C., Li, Q. & Zhang, L. (2012), ‘An efficient backward euler time-integration method for nonlinear dynamic analysis of structures’, *Computers & structures* **106**, 20–28.
- Lyashko, A. & Solov’Yev, S. (1991), ‘Fourier method of solution of fe systems with hermite elements for poisson equation’, *Russian Journal of Numerical Analysis and Mathematical Modelling* **6**(2), 121–130.
- Matthews, A. P. (1994), ‘Current advance method and cyclic leapfrog for 2d multi-species hybrid plasma simulations’, *Journal of Computational Physics* **112**(1), 102–116.
- Merle, F. & Zaag, H. (2000), ‘A liouville theorem for vector-valued nonlinear heat equations and applications’, *Mathematische Annalen* **316**(1), 103–137.
- Mikkola, S. & Aarseth, S. (2002), ‘A time-transformed leapfrog scheme’, *Celestial Mechanics and Dynamical Astronomy* **84**(4), 343–354.
- Pramanick, S. (2020), ‘Onsets and outflow distributions in abelian and stochastic btw models’, *arXiv preprint arXiv:2009.04516* .
- Pramanick, S., Dey, A. & Chandra, S. (2020), ‘Electron-acoustic solitary waves in fermi plasma with two-temperature electrons’, *DOI: 10.2139/ssrn.3711910* .
- Rice, J. R. (1960), ‘Split runge-kutta method for simultaneous’, *Journal of Research of the National Bureau of Standards: Mathematics and mathematical physics. B* **64**, 151.
- Sahana, S., Mitra, S., Chandra, S. & Pramanick, S. (2021), ‘Linear properties of electrostatic wave in two-component fermi plasma’, *arXiv preprint arXiv:2101.00510* .

- Shampine, L. F. (2009), ‘Stability of the leapfrog/midpoint method’, *Applied mathematics and computation* **208**(1), 293–298.
- Skeel, R. D. (1993), ‘Variable step size destabilizes the störmer/leapfrog/verlet method’, *BIT Numerical Mathematics* **33**(1), 172–175.
- Skölleremo, G. (1975), ‘A fourier method for the numerical solution of poisson’s equation’, *Mathematics of Computation* **29**(131), 697–711.
- Xiong, X., Chen, W., Jin, S. & Kamal, S. (2019), ‘Discrete-time implementation of continuous terminal algorithm with implicit-euler method’, *IEEE Access* **7**, 175940–175946.